1-24-2024

Evaluating A Satellite Passive Microwave Snowmelt Detection Algorithm Using In-Situ Snowmelt Indicators

Angela Rienzo
Syracuse University

Abstract

Snowmelt is a critical component of hydrologic processes in mountainous and seasonally cold regions. As such, monitoring and understanding regional snowmelt patterns and fluctuations is a crucial aspect of water resource management. While ground-based snow monitoring stations can provide continuous data on melting processes, they are cost-prohibitive for dense coverage at regional to global scales. Satellites, however, can provide global data on weekly to twice daily time scales. Previous studies have found that passive microwave (PMW) remote sensing data from satellites with twice daily observations can be used to detect onset of snowmelt using changes in brightness temperature (a measure of emitted radiation) from day to night, known as the diurnal amplitude variation (DAV). This study first evaluates the accuracy of an enhanced DAV method developed by Tuttle & Jacobs (2019) in a heterogenous environment consisting of forest and cropland by comparing satellite detected melt events to detailed ground snow observations collected at Sleeper's River Research Watershed, VT between 2021-2023. Using lessons learned, the analysis is extended to over 500 snow stations located throughout the western US and Canada, using daily SWE and snow depth data from 2002-2011. This study aims to fill gaps in 1) evaluating PMW melt detection techniques using detailed observations of the snowpack energy state, and 2) assessing their performance in mid-latitude regions and a variety of different terrains/climates. I find that snow surface temperature observations are more valuable than other tested methods for validation of melt events detected using PMW observations. I also find that, in accordance with previous studies, PMW melt detection methods are likely most sensitive to liquid water at the surface of the snowpack, making them more useful for detecting midwinter surface melt and the onset of the spring melt period, rather than hydrologically significant releases of snowmelt.

EVALUATING A SATELLITE PASSIVE MICROWAVE SNOWMELT DETECTION ALGORITHM USING IN-SITU SNOWMELT INDICATORS

by

Angela Rienzo

B.S., Hofstra University, 2020

Thesis
Submitted in partial fulfillment of the requirements for the degree of
Master of Science in Earth Sciences

Syracuse University
December 2023

Acknowledgements

I am extremely grateful to my advisor, Dr. Sam Tuttle, who has provided unwavering guidance and support, both in my research and as an overall scientist. I would not have been able to achieve all that I have without his mentorship, expertise, and patience. I'd like to thank my collaborators, Dr. Carrie Vuyovich, Dr. Elias Deeb, and Dr. George Duffy for their support and mentorship, as well as committee members Dr. Elizabeth Carter and Dr. Tao Wen for their constructive feedback and guidance throughout my time in this department. I'd also like to thank fellow graduate students Haejo Kim, Madison Woodley, and Tyler Logie, who have provided fieldwork assistance, intellectual support, and ongoing encouragement.

Research at the Sleeper's River Research Watershed field site would not have been possible without assistance from Dr. Dave Chandler and the USGS. I would like to specifically acknowledge USGS scientists Jamie Shanley and Serena Matt for providing support in the setup and ongoing operation of our field research site. I would also like to thank Dr. Eric Kelsey for allowing us to use custom built field equipment that were vital in field data collection.

I would like to acknowledge NASA, Syracuse University, and the Department of Earth and Environmental Sciences for ongoing financial support for my research.

Finally, I'd like to thank my friends and family for their ongoing support throughout my time in Syracuse. I would not have made it this far without them.

Table of Contents

1. Introduction

Snowmelt is an integral component of both the hydrologic cycle and energy budget for seasonally cold regions. Many rely on seasonal spring snowmelt to replenish local reservoirs, rivers, and aquifers for drinking water, agriculture, and recreational activities. In mountainous regions, snowmelt can account for as much as 80% of the total annual runoff (Li et al., 2017). Snowmelt has become especially important in recent years as extreme droughts become more common, resulting in low water storage in surface and subsurface reservoirs and decreasing snowpack accumulation in the winter (Barnett et al., 2005; Musselman et al., 2021). With rising global temperatures, spring snowmelt rates are projected to decrease, resulting in decreased runoff and streamflow for many water stressed areas (Musselman et al., 2017). Warmer temperatures are also likely to bring more midwinter melt events, such as rain-on-snow (Putkonen et al., 2009), and cause overall shifts in spring melt timing (Adam et al., 2009; Clow, 2010; Stewart, 2009).

Snowmelt is also an important factor to consider in flood hazards during the winter and spring months for many northern regions. Rapid snowmelt rates can cause a high volume of runoff into streams over a short period of time, resulting in flooding that can negatively impact downstream communities. This hazard may be further amplified by increasing temperatures and frequency of rain-on-snow events due to climate change (Freudiger et al., 2014; Musselman et al., 2018). The resulting floods can have destructive societal impacts, as well as ecological and geological consequences, and therefore it is important to predict and understand how the hydrological drivers may change with shifting climates. Monitoring snowmelt in these areas could help to predict flooding hazards and water availability for snowmelt-dominated watersheds.

1.1 Background

1.1.1 Snowpack Dynamics

A snowpack is a very dynamic and heterogeneous system that undergoes constant change. Newly fallen snow is made up of ice crystals, air, and sometimes liquid water within its pore spaces. The ice crystals can vary in size, density, and liquid water content (or "wetness") due to factors such as atmospheric temperature humidity during formation, surface wind speed, and air temperature during precipitation (Mellor, 1964). These factors can vary significantly between precipitation events, resulting in a buildup of semi-homogenous horizontal layers of snow with varying crystal sizes (or "grain sizes") and densities. Newly fallen snow immediately experiences density adjustments due to initial gravitational settling, while deeper layers experience densification from compaction. The ice crystals in these layers experience different types of metamorphism throughout the winter, such as sublimation and redeposition of ice within the snowpack, as well as melting and refreezing. These processes cause further changes in snow grain size and shape, density, and wetness throughout the winter.

Regions that experience seasonal snow, or snow that does not last for more than a year, tend to follow general seasonal patterns of snow accumulation and melt, shown in Figure 1. The accumulation period typically occurs in the first half of the season, when the amount of snow on the ground is increasing. The melt, or ablation, period occurs late in the season and consists of three subphases: warming, ripening, and output phases. Snowpack temperatures are always at or below 0°C. Once the snow reaches 0˚C, any additional net input of energy will cause melting. The melt phase begins when the total energy input into the snowpack outweighs the energy output, causing the snow to warm until it is isothermal, or 0°C throughout the snowpack. The ripening

phase begins at the start of melting, but meltwater stays trapped within the snowpack due to surface tension. At this stage, the snowpack consists of solid ice, liquid water, and air. The amount of liquid water contained in the snowpack is also known as liquid water content (LWC), and snowpack that contains liquid water is termed "wet". The output phase begins when the snowpack cannot hold any more liquid water due to surface tension and further energy inputs result in water leaving the snowpack (Dingman, 2014). This output phase is considered to be hydrologically significant, as water is leaving the snowpack. It is also important to note that many snowpacks do not exactly follow this paradigm. Shallower snowpacks are more sensitive to changes in weather due to relatively lower thermal inertia, which can cause midwinter surficial melt events with slight increases in air temperature or solar radiation.

1.1.2 Snowpack Measurement Techniques

There are many different techniques for measuring a wide range of snow properties on various spatial and temporal scales. These can be either destructive or nondestructive to the snowpack, automated or manually collected, in situ or remotely sensed, and representative of a wide range of spatial scales, from a single point to areal averages over many kilometers. There are also many different techniques that can be used to collect the same type of measurement. The most common snow measurements include snow depth, or the height of the snowpack from the ground, and snow water equivalent (SWE). SWE is the depth of liquid water contained in the snowpack if it were to completely melt. A decrease in SWE indicates that water has been lost from the snowpack, most likely due to melting, making this measurement vital for forecasting water availability and timing from spring snowmelt runoff in mountainous regions. Manual data collection usually consists of measuring the mass, volume, and depth of the snow to calculate SWE. Manual SWE measurements require collecting a core of snow, typically in a standard

volume snow tube, with a record of the depth, volume, and weight of the sample. A "snow pillow" is common alternative that uses a fluid-filled pad with an internal pressure sensor under the snowpack to allow for continuous observations of SWE based on its mass. Analogous sensors have been developed that use a load cell instead of a fluid-filled pad, called "fluidless snow pillows" or "snow scales".

Snow depth is another potential indicator of snowmelt, as a decrease in snowpack height can indicate that some type of melt has occurred. Manual snow depth can be collected using a snow depth probe or ruler. One technique for continuous snow depth measurements is to use a time lapse camera to take photographs of the height of the snowpack around a stationary graduated snow depth stake or ruler. Snow depth can then be extracted manually though human observation, or through advanced automated extraction techniques (Kopp et al., 2019). More precise automated snow depth measurements can be obtained using ultrasonic sensors mounted above the snowpack that determine the distance from the sensor to the snow surface, which allows for calculation of the height of the snowpack (Kinar & Pomeroy, 2015).

Although both SWE and snow depth are commonly used for snowmelt monitoring, there are many more processes that can affect both measurements other than melting, making them imperfect melt indicators. For example, sublimation and wind redistribution of the snowpack can cause a decrease in SWE and snow depth even if melt is not occurring. Snow depth also naturally decreases over time due to compaction and deformation of deep snow layers under pressure. Rapid compaction commonly follows snowfall events due to the gravitational settling of fresh snow. Decreases in snow depth may also indicate different types of snowmelt events besides pure loss of water from the snowpack, such as melt-refreeze events. These occur when certain melting snow is refrozen before any water is lost from the snowpack, usually causing densification of the snow and

a decrease in snow depth. These types of melt events are common throughout the mid-winter season, as snowpack temperatures warm during peak solar radiation at midday, before quickly falling during the evening and refreezing any liquid water. While these conventional snowpack measurements are useful for tracking physical changes in the snowpack, they lack insight into the thermodynamics, energy balance, and vertical and horizontal variability of snow.

1.1.3 Remote Sensing

Another popular but destructive field technique for understanding vertical variability within deep snowpacks is a snow pit. This method involves digging a pit in the snowpack with at least one vertical, flat wall that extends from the top of the snowpack to the ground (Fierz et al., 2009). A multitude of measurements and observations may be taken along the vertical transect of the snowpack to understand the spatial variability and snow metamorphism. The most common data collected in snow pits are density, temperature, grain size and shape, and snow water equivalent (SWE) (Kinar & Pomeroy, 2015). Besides snow researchers, this method is also very popular with snow recreationists as a means to assess the risk of avalanches due to instabilities in the snowpack created by differences in snow density and grain types within layers (Schweizer et al., 2021). While snow pits provide a wealth of data and insight, they are very time consuming for results valid only at a one point in space and time, and their measurements can be subjective and overall destructive of the snowpack (Kinar & Pomeroy, 2015).

Thermal snow measurements can provide an understanding of the energy state and energy transport within the snowpack. Specifically, measuring the vertical temperature gradients can provide information on the potential for melt and ice crystal metamorphism within the snowpack. Although there is a lack of commercially designed and produced instruments for this type of

automated temperature measurements, there have been numerous studies published since at least 1944 using a variety of designs for continuous vertical snowpack temperature measurements (R. W. Gerdel, 1944). Some structures use sensors strung along horizontal wires to largely avoid disturbing snowfall patterns (Helgason & Pomeroy, 2012; Sturm & Johnson, 1991). Other designs use sensors mounted along a vertical solid stake or "ladder", which allows for better durability throughout the winter, but have a large impact on the surrounding snowpack (Ingólfsson et al., 2012). Most designs, however, fail to eliminate the effect of preferential melting around these devices, causing a similar affect to tree wells (McGurk, 1983). A wide range of sensors have also been used, weighing factors such as cost, size, data storage, Bluetooth connectivity, and overall durability in wet, freezing conditions.

The temperature of the snow surface can also provide valuable insight into energy exchange and melt processes. Ground-based infrared radiometers, also known as infrared "thermometers", measure longwave radiation emitted from a target surface. These measurements can also be supplemented by the use of pyrgeometers, which measure background radiance, to apply corrections for ambient radiation. This technique has been used in multiple studies to provide automated, non-destructive snow surface temperature observations for ground validation of satellite products (Pérez-Díaz et al., 2017).

In-situ snow measurement sites can monitor high-resolution temporal variability in snow properties; however, each only provides site-specific data that is only representative of a limited surrounding area (Blöschl, 1999; Meromy et al., 2013). For large scale studies, researchers can use satellites and airborne sensors for continuous snow observations. While satellites have coarser spatial resolution than ground-based observations, and thus cannot observe small-scale variability, many satellites observations are freely accessible and allow for global scale observations. Satellite

and airborne remote sensing observations are also the least destructive to snowpacks compared to most ground-based measurement techniques. Visible and infrared satellite observations have been used for snow studies, specifically looking at properties such as snow cover extent and reflectivity from surface albedo (Frei et al., 2012). One of the largest issues with optical sensors, however, is the sensitivity of this range of the electromagnetic spectrum to cloud cover, sunlight, and vegetation. Microwave observations have greater potential for snow observations partly due to its ability to penetrate through clouds and snowpack on the ground, along with its sensitivity to snowpack properties and subsurface features (Hallikainen et al., 2018). Active microwave satellites, such as Sentinel-1, provide high resolution observations of up to 10 m, but have return frequencies between 2-14 days depending on latitude. Passive microwave satellites, such as SSM/I, SSMIS, AMSR-E, and AMSR2, offer twice daily data with native resolutions between 5-50 km. These sensors detect microwave radiation naturally emitted by a target (e.g., a location on Earth), compared to active sensors which emit radiation to a target and measure the amount of energy returned (backscatter) and return time. Because Earth's surface emits microwave radiation at very low intensity, larger footprints are necessary for the radiation to be detectable by the satellite, resulting in decreased resolution compared to active sensors. PMW satellites also typically measure radiation at various channels between 1-89 GHz.

Passively emitted microwave radiation, as measured by a radiometer, is typically expressed as brightness temperature (T_b), and is approximated based on the Rayleigh-Jeans approximation:

Equation 1: $T_b = \varepsilon * T_s$.

In this equation, ε is emissivity and T_s is the physical temperature (K). Physical temperature includes anything within view of the satellite that emits microwave radiation, including the atmosphere, vegetation, snow, and ground. Because liquid water has a much higher dielectric

constant than a dry (i.e., completely frozen) snowpack, a wet snowpack will result in significantly higher emissivity compared to a dry snowpack (Stiles & Ulaby, 1980). When using AMW or PMW observations to measure snow properties such as depth, SWE, and extent, the presence of liquid water dominates the microwave signal and causes errors in algorithms that rely on the scattering and radiative properties of dry snow (Conde et al., 2019; Dong et al., 2005; Tanniru & Ramsankaran, 2023).

Most snowmelt events tend to occur during the day, when solar radiation and, usually, air temperature peak. Ramage & Isacks (2002) calculated the difference in brightness temperature from day to night, which they termed the diurnal amplitude variation (DAV), to detect melt events. Similar DAV methods were later adopted by (Tedesco, 2007). Calculations of DAV require two satellite passes over the same location: one during nighttime and another during daytime. If the brightness temperature significantly increases between a consecutive nighttime and daytime satellite pass, this indicates liquid water is present during the daytime and melting has occurred. Since this method calculates relative diurnal change, it will only detect water phase changes, rather than continuously wet snow. A continuously wet snowpack will only show a melt event at the first time-step when liquid water was present (Tuttle & Jacobs, 2019). Therefore, DAV methods are best for detecting melt event onset rather than the duration of melt events.

Although past studies have shown that PMW DAV algorithms contain valuable information about snowpack energy processes and transitions, they do not account for the influence of physical temperature (T_s) on brightness temperature (T_b), as shown in equation 1. Tuttle and Jacobs (2019) attempt to account for the influence of physical temperature changes using an enhanced DAV method called ΔT_b-ΔT_a. In this method, diurnal changes in air temperature, ΔT_a (as a proxy for T_s), are plotted against coincident diurnal brightness temperature

changes, ΔT_b. They found that for frozen snow, the two show a roughly linear relationship, and that T_b changes which are much larger than what would be expected from the linear ΔT_b-ΔT_a relationship can be classified as melt and refreeze events (Figure 1), as they are assumed to be a result of water phase changes that change the emissivity of the snow.

1.2 Research Questions and Hypotheses

The goal of this research is to evaluate the usefulness of passive microwave (PMW) satellite data for detecting snowmelt events, and to investigate the utility of different types of in-situ snow observations for validation. Many methods have been established using PMW data to detect snowmelt (Abdalati & Steffen, 1995; Apgar et al., 2007; Dolant et al., 2016; Foster et al., 2011; Grenfell & Putkonen, 2008; J. M. Ramage & Isacks, 2002; Tedesco et al., 2009; Tuttle & Jacobs, 2019; Walker & Goodison, 1993; Zheng et al., 2018), and microwave emission modeling studies suggest that PMW techniques are sensitive to very small amounts of liquid water in the snowpack (Chang et al., 1987; Mätzler, 1987; Stiles & Ulaby, 1980). However, the accuracy of PMW snowmelt detection methods, with respect to ground-based observations, has not been well established. In fact, it is not definitively known what character of snowmelt the satellites are sensitive to (e.g., melt only at the snow surface, or melt throughout the entire snowpack).

The first part of this study assesses the utility of a modified version of the ΔT_b-ΔT_a PMW satellite melt detection algorithm in a heterogenous domain consisting of forest and cropland using a variety of in-situ snow measurements collected at Sleeper's River Research Watershed (SRRW) in Northeastern Vermont. Based on the sensitivity of passive microwave brightness temperature to liquid water in the snowpack, the ideal ground indicator for validation would be liquid water content of the snowpack. However, these data are very rare and difficult to collect autonomously.

Therefore, I compare the physical conditions within the snowpack to satellite snowmelt signals I aim to determine **1) the ability of the satellite to detect radiative fluxes in the snowpack**, and ***2*) which in-situ melt indicator is most ideal for this analysis based on the sensitivity of the algorithm to certain snowpack processes**. In-situ melt indicators include snow depth decreases, internal snowpack temperature, and snowpack surface temperature. I hypothesize that the thermal melt indicators will have the best agreement with the satellite melt algorithm, as they are a better indicator of the presence of liquid water in the snowpack compared to snow depth.

In the second part of the analysis, I extend the study to the western US using standard daily snow depth and SWE measurements from SNOTEL stations to **1) determine if widely available data such as snow depth and SWE are appropriate melt indicators** and **2) assess the performance of the ΔT_b-ΔT_a method at a regional scale and detect potential relationships with certain land and snow characteristics.** Since most snow stations only measure snow depth and SWE, these are the only in-situ melt indicators tested for this regional study. I hypothesize that neither will prove to have high agreement with the satellite algorithm, as neither are direct proxies for detecting energy transfer within the snowpack.

The environmental conditions in different regions (e.g., climate, land cover type, elevation) lead to distinct snowpack characteristics, such as typical snow amount and persistence, which in turn lead to different spatial and temporal patterns of melt. It is unclear how well the PMW satellites can detect snowmelt events under different environmental conditions, such as if there is a thick tree canopy over the snowpack (Serreze et al., 1999; Walker & Goodison, 1993), or the depth at which microwave radiation becomes saturated and undetectable by the PMW satellite instrument (Chang et al., 1976; Dong et al., 2005; Foster et al., 2005). Therefore, this analysis will also explore how well satellites can detect snowmelt in areas with varying snow and land

characteristics, such as annual maximum snow depth/SWE, tree cover fraction, elevation, and snow class (Sturm & Liston, 2021). In general, I expect to see poorer agreement with higher tree cover fraction due to attenuation of the microwave signal. I also expect to see worse agreement at sites with higher annual maximum snowpack due to potentially incomplete penetration of the microwave radiation through the snowpack (Stiles & Ulaby, 1980) and larger energy requirements for melting deeper snowpacks.

Given that DAV methods use changes in brightness temperature to detect melt, only the initial transitions from dry to wet snow (and refreezing from wet to dry) should be detectable using these methods. Consecutive observations of wet snow should produce similar brightness temperatures (after accounting for changes in physical temperature), which would show no change and therefore no melting events. I hypothesize that the ΔT_b-ΔT_a method is most useful for detecting melt/refreeze events and melt onset, while it is less useful for detecting hydrologically significant melt events that would release water from the snowpack.

1.3. Study Site for Part 1: SRRW Analysis

Sleeper's River Research Watershed (SRRW) is a USGS/USDA snow and hydrology research site that has been in operation since 1958. The watershed encompasses 287 km^2 of mixed deciduous and coniferous forest and agricultural land in Northeastern Vermont **(**Figure 2), with an elevation range of 213-762m. The watershed drainage flows from northwest to southeast, from Pope Brook draining into Sleeper's River and eventually into the Connecticut River. Relevant research conducted in the watershed includes the effect of frost depths on snowmelt runoff and recharge (Shanley & Chalmers, 1999), the effects of snowmelt timing and shifts on the chemistry of surface waters (Porter et al., 2022), and snow energy balance modeling and soil temperature

simulations (Sun & Chern, 2005). There have also been weekly snow depth and SWE field sampling measurements taken throughout the watershed since 1960.

In Fall of 2021, Sam Tuttle's research group began setting up a variety of automated snow measurement instruments at the SRRW snow research site (44.482942˚ -72.164879˚) located just north of Danville, VT at an elevation of 554m. Data were collected for the 2021-2022 and 2022-2023 winter seasons. Instruments include a Sommer Messtechnik Snow Pack Analyzer 2, various vertical profiles of snowpack temperature, an infrared radiometer, and a snow depth stake and time lapse camera (Figure 3, Table 1). This location also houses an active weather station and fluidless snow pillow run by the USGS and the University of Vermont, which was installed in winter 2022-2023. While these data were not available at the time of this study, future research efforts at this site could explore the possibility of collaboration and data sharing.

2. Data

2.*1 Satellite Data*

2.1.1 Part 1: SRRW Analysis

The first part of this analysis (hereafter the "SRRW analysis"), I applied the ΔT_b-ΔT_a PMW melt detection method at SRRW. The PMW data used in this method are Level 3 T_b from the Advanced Microwave Scanning Radiometer 2 (AMSR2) instrument aboard the Japanese Aerospace Exploration Agency (JAXA) GCOM-W1 satellite, at the native 25km spatial resolution. Observations from the vertically polarized 37 GHz frequency were used as it has been shown to be the most sensitive to liquid water in the snowpack (Stiles & Ulaby, 1980) and has been used in many similar studies (Apgar et al., 2007; J. M. Ramage & Isacks, 2002; Tuttle & Jacobs, 2019;

Zheng et al., 2018). AMSR2 began collecting data in 2012 and is still in operation. In this analysis, I use data for two winters (2021-2022 and 2022-2023), coincident with ground observations at SRRW. AMSR2 has two overpasses per day, approximately 12 hours apart, with an equatorial local overpass time of 1:30pm ascending and 1:30am descending.

2.1.2 Part 2: SNOTEL Analysis

The second part of the analysis (hereafter the "SNOTEL analysis"), I applied the ΔT_b-ΔT_a PMW melt detection method at over 500 snow monitoring stations in the western U.S. The PMW data used in the method are the MEaSUREs Calibrated Enhanced-Resolution Passive Microwave Daily EASE-Grid 2.0 Brightness Temperature ESDR for the Advanced Microwave Scanning Radiometer for EOS (AMSR-E) instrument aboard the NASA Aqua satellite (Brodzik et al., 2016). AMSR-E was operative from 2002 to 2011, and I use the data for all winters between August 2002 to August 2011. These data have the same overpass times, spatial resolution, electromagnetic frequency, and polarization as AMSR2.

2.2 In-Situ Data from SRRW

A summary of ground-based instrument data availability for the SRRW site for winters 2021-2022 and 2022-2023 can be found in Figure 4.

2.2.1 Snow Pack Analyzer-2

The Snow Pack Analyzer-2 (SPA-2) measures the volume content of ice, water, and air within the snowpack. Flat sensor bands running horizontally at 10 and 30 cm above the ground and one running diagonally through the snow can distinguish between these components by measuring the complex impedance the sensor at two different frequencies. The SPA-2 also

includes an ultrasonic snow depth sensor, which measures the return time of a sonic pulse reflected off of the snow surface to infer snow depth, with a 1mm resolution and 0.1% accuracy. The final products that can derived include SWE, liquid water content (LWC), ice content, and snow density at 10-minute timesteps. Due to issues with calibration of the sensor bands, only the snow depth data are available at this time. Since this instrument was initially installed midwinter of 2022 and required widespread disturbance of the snowpack, so only snow depth data from winter 2022-2023 are used in this study.

2.2.2 Snow Depth Stake & Timelapse Camera

To supplement the snow depth sensor, a Wingscapes Timelapse Pro camera and graduated snow depth stake were installed for both winter seasons. The camera recorded photographs of the snow depth stake and surrounding instruments every hour for the full snow season. This allowed us to reconstruct a time series of snow depth, and also determine if/when instrumentation became physically degraded/damaged or if the snowpack was unnaturally disturbed throughout the winter. These snow depth data for winter 2021-2022 were used in this analysis.

2.2.3 Vertical Temperature Profiles

Three different vertical temperature profile (or "temperature ladder") configurations were used at SRRW to measure the temperature dynamics of the snowpack. The different temperature ladder constructions were used to test which sensors and/or configurations worked best in harsh winter conditions. Two of the ladders included Bluetooth enabled HOBO MX2201 Water Temperature Data Loggers and iButton DS1922L Temperature Data Loggers, respectively, mounted onto either wooden or PVC stakes. The third ladder was a custom-made thermistor ladder provided by Eric Kelsey (Plymouth State University), which consisted of Campbell Scientific

thermistor beads heat shrink wrapped onto long spindles and wired to a Campbell Scientific data logger (hereafter referred to as the "custom ladder"). All temperature ladders recorded temperatures every 10 cm from the ground (up to at least +90 cm). The HOBO and custom temperature ladders collected data at 10-minute intervals, while the iButton ladders collected data at 1-hour intervals due to limited internal data storage. Due to programming issues, the custom ladder was not able to collect data during Winter 2021-2022. Data are also unreliable for both the HOBO and iButton temperature ladders for Winter 2022-2023 due to damage and dislodging of sensors that occurred midwinter during a period of heavy snowpack.

2.2.4 Infrared Radiometer & Pyrgeometer

Prior to winter 2022-2023, an Apogee SI-111-SS infrared radiometer sensor was installed to observe the surface temperature of the snowpack. This instrument measures infrared radiation in an 8-14 um wavelength range (also known as "longwave" radiation) emitted from the underlying surface (snow or bare ground), in combination with downwelling longwave radiation reflected off of the surface. The amount of longwave radiation emitted from an object (e.g., snow) is a function of its temperature and emissivity, according to the Stefan Boltzmann Law. In order to get an accurate snow surface temperature, an emissivity correction must be applied, and the reflected background longwave radiation must be accounted for. Therefore, an Apogee SL-510-SS upward-looking pyrgeometer sensor was also installed midwinter on February 7th in 2023. The data were collected at 10-minute intervals.

2.3 SNOTEL Data

In-situ data from the Snowpack Telemetry Network (SNOTEL), which has over 900 automated snow monitoring stations across the western US, were used to evaluate the satellite-derived melt events in the second part of this study. Most SNOTEL stations measure and report daily SWE, snow depth, and maximum and minimum air temperature, which are available on the US Department of Agriculture (USDA) Natural Resources Conservation Service (NRCS) National Water and Climate Center (NWCC) website. Snow depth is measured using ultrasonic sensors that sit above the snow and measure the return time of a sonic pulse reflected off the snow surface. Temperature data are collected using a shielded thermistor located at least 2 meters above the ground. SWE is measured using snow pillows, which are located under the snowpack and measure the weight of the overlying snow. Snow depth and temperature data were downloaded directly from the SNOTEL website, while SWE was gathered from a more extensive dataset from Musselman et al. (2021). This latter dataset includes SWE from SNOTEL and other networks, such as in California and Canada, and it has been thoroughly QA/QC'ed. All data were gathered from stations in the contiguous U.S. for October 1, 2002, to September 30, 2011 (coincident with the AMSR-E satellite instrument), resulting in 563 sites with SWE, 481 sites with snow depth and temperature, and 444 sites with all three measurements.

2.4 Snow Class Data

Snow climate classes over North America from Sturm et al. (2021)**,** as seen in Figure 5, were used to examine differences in snowmelt between SNOTEL sites. The data were downloaded as a GeoTIFF file at 300m spatial resolution. This map classifies the snowpack into different categories according to air temperature, precipitation, and wind speed. Each category is meant to

represent a unique set of shared snowpack characteristics such as snow depth, density, texture, and layering. Using ArcMap 10.8.1, the snow class for each SNOTEL station was extracted from the GeoTIFF dataset using the station's latitude and longitude. The total number of stations within each snow class can be seen in Figure 6. Based on the original classification, there are 7 total snow classes, but no stations in this study were found to be classified as “Ice”. There are also very few snow stations in areas with ephemeral snow, where snowpack does not always persistent throughout the winter.

2.5 Tree Cover Data

Forest fraction, or the percentage of a pixel covered by trees during peak foliage, has been shown in previous studies to have an impact on the ability of a satellite to accurately observe ground conditions (Foster et al., 1991). A global tree cover fraction dataset was downloaded from Hansen et al. (2010) at 30m resolution. Tree cover fraction was extracted for each snow station location. Average tree cover fraction was also calculated for each 25km AMSR-E satellite pixel in order to investigate the potential effects of tree cover on the satellite data.

3. Methods

A summary of all melt detection indicators and instruments used for each part of this analysis can be found in Table 1.

3.1 Satellite Melt Detection

The AMSR-E and AMSR-2 satellite data were processed identically for all analyses using a modified version of the ΔT_b-ΔT_a melt detection method from Tuttle & Jacobs (2019). The

detection algorithm was restricted to only include times with snow on the ground based on in-situ snow depth data. In this method, 12-hourly changes in brightness temperature (ΔT_b) are paired with coincident air temperature changes (ΔT_a). In this analysis, we use NLDAS-2 air temperature data (Mitchell et al., 2004). Tuttle & Jacobs (2019) found that when the snow is completely frozen, ΔT_b and ΔT_a form a roughly linear relationship, which can be approximated by a linear regression. This represents the expected change in brightness temperature observed by the satellite from a given change in air temperature (which is a used as a proxy for physical temperature; see Equation 1). In the original paper, melt and refreeze events were classified as observations that fell more than 10 K from the ΔT_b-ΔT_a regression line. In subsequent investigations, it was found that the ΔT_b-ΔT_a slope varies by location (due to different land surface characteristics, snow dynamics, etc.), which means that a 10 K threshold may not be appropriate everywhere. A method called k-means clustering, a form of vector quantization, was instead used to detect which observations significantly deviated from the ΔT_b-ΔT_a line (Figure 7). Using k-means clustering, the ΔT_b residuals from the regression line were classified into three groups: melt events (strongly positive residuals), freeze events (strongly negative residuals), and non-events (residuals close to zero). This method is adaptable to different locations and hypothetically allows for a more accurate identification of melt events than assuming that a constant threshold applies everywhere.

After applying the ΔT_b-ΔT_a method, the resulting datasets of melt events contained twice-daily data for each pixel. Satellite-detected melt events were assigned a value of 1, 0 indicated no melt event, and NA indicated missing or removed data.

For part 1 of this study (SRRW Analysis), a time series of 12-hourly ΔT_b-ΔT_a snowmelt events was produced for the AMSR2 pixel containing our field site location at SRRW for November 1, 2021, through May 24, 2023, corresponding with ground-based data collected at the

site. The ΔT_b-ΔT_a line used to identify these events was fit to all 12-hourly AMSR2 ΔT_b and NLDAS-2 ΔT_a data with snow cover from September 1, 2012, to May 31, 2023. For winters 2021-2022 and 2022-2023, this was observed snow cover at the SRRW site, and for all prior winters only data from December and March were included in the analysis.

For part 2 of this study (SNOTEL Analysis), ΔT_b-ΔT_a snowmelt events were identified for the AMSR-E pixels containing the locations of the SNOTEL stations, resulting in a 12-hourly time series of snowmelt events for each station from August 1, 2002, to July 31, 2011 (9 winters). The 12-hourly melt event data were then degraded to a daily timestep for better comparison with the daily SNOTEL ground data. To create the daily dataset, any day with at least one melt event detected (out of the two 12-hourly timesteps) was designated as a melt event.

For simplicity, references to the ΔT_b-ΔT_a melt indicator will herein be referred to as the "satellite" melt indicator.

3.2 SRRW In-Situ Melt Indicators

For part 1 of this analysis, different in-situ melt detection indicators were derived from detailed ground snow data collected at Sleeper's River Research Watershed to evaluate the satellite melt detection methods.

3.2.1 Internal Snowpack Temperature

One way to determine if snow is melting or contains liquid water is to measure the vertical temperature profile of a snowpack. Theoretically, if the entire snowpack reaches 0°C, the snow is isothermal, or ready to melt. In winter 2022-2023, the custom thermistor temperature ladder data were used to determine when the snowpack became isothermal. In winter 2021-2022, the iButton

and HOBO temperature ladder data were used. The mean temperature was calculated for sensors under the snowpack, starting at 10cm above the ground. Data from sensors that were less than 10cm from the top of the snowpack were removed to limit the influence and exposure of solar heating and radiation to due to significant welling observed around the instrument (McGurk, 1983). Snow depth data from the SPA-2 was used to constrain these heights, with a matching temporal resolution of 10 minutes. A melt event was then detected if any of the average snowpack temperatures within the same 2-hour window around the satellite overpass reached -0.1 C. This indicates the snowpack has reached or is approaching isothermal, which is when a large melt event is most likely to occur.

3.2.1 Surface Temperature

In winter 2022-2023, the surface temperature of the snowpack was also used as a thermal melt indicator, as it can provide unique insight into surface melt caused by solar radiation. Surface temperature was derived from the infrared radiometer sensor (IRT), using the pyrgeometer background reflectance data to correct for surface emissivity (Equation 2).

$$\textbf{Equation 2: } T_{Target} = \sqrt[4]{\frac{{T_{Sensor}}^4 - (1-\varepsilon)\cdot {T_{Background}}^4}{\varepsilon}}$$

In this equation, the T_{Target} is the actual temperature of the surface, T_{Sensor} is the brightness temperature measured by the IRT, $T_{Background}$ is the background brightness temperature measured by the pyrgeometer, and ε is the emissivity of the surface. Brightness temperatures from the IRT and pyrgeometer are outputs from the instruments, which use a modified Stefan-Boltzmann equation for internal calibration (Apogee, 2015). Emissivity of the snow surface was assumed to be 0.98, as typical ranges for snow have found to be 0.97-0.99 (Dozier, 2011; Hori et al., 2013).

The surface temperature data were restricted to only data within +/- 1 hour of the satellite overpass times (1:30am and 1:30pm local time). A melt event occurred if any of the 10-minute temperature readings from this window approached 0 (> -0.1°C), indicating the surface of the snow was approaching the point at which it could melt.

3.2.3 Snow Depth

Since continuous thermal snowpack observations are uncommon, snow depth was also investigated for its use as a melt event indicator. For 2023, 12-hourly snow depth data were extracted from the SPA-2 snow depth dataset for the corresponding AMSR-2 satellite overpass times. SPA-2 snow depth data are not available for the winter of 2022 due to mid-winter installation of the instrument that caused snow disturbance, so snow depth was instead visually determined using 12-hour camera photographs of the snow depth stake at the site. This also introduced a higher level of human error and less precision, especially due to visual effects by the snow camera angle, disturbed snow, and welling around the snow stake. The difference in snow depth was then calculated to determine when the snow depth was decreasing, and therefore potentially experiencing a melt event. The threshold to indicate a melt event was set at less than or equal to -1cm (i.e., at least 1cm of snow depth decrease).

3.3 SNOTEL In-Situ Melt Indicators

For part 2 of this analysis, snow observations made abundant by extensive snow monitoring networks were used as melt indicators to evaluate the satellite melt detection method at a wide range of locations and environments over a 9-year period.

3.3.1 Snow Depth

Similar to the SRRW analysis, snow depth was used as a melt indicator for the large-scale analysis of SNOTEL sites, but instead using the publicly available and QA/QC'd daily data. Because air temperature was available at these sites, days with decreasing snow depth were not considered melt events unless the daily maximum air temperature exceeded 0°C, to limit the influence of potential confounding factors such as compaction, wind redistribution, or sublimation. A threshold of at least -2 cm (instead of the -1 cm threshold used for SRRW) was used to the longer timestep (daily, as opposed to 12-hourly for SRRW).

3.3.2 SWE

I also investigated SWE for use as a melt event indicator due to the abundance of measurements in comparison to other snow observations. While SWE data from the SPA-2 was not yet available for use at the SRRW site, daily SWE data were used for the analysis of SNOTEL stations across the western U.S. Processing was almost identical to that for the SNOTEL snow depth data, except a threshold of -2 cm ΔSWE was used to indicate a melt event and was not temperature restricted.

We expect that most SWE decreases are due to melting that leads to loss of water from the snowpack, but it is also possible to lose snow mass via blowing snow or sublimation. However, SWE is not sensitive to melt/refreeze events that do not change the overall mass of water in the snow, and thus may not be an ideal ground truth for PMW melt detection methods, which are sensitive to snow liquid water content. Alternatively, melt events detected by decreases in SWE may not be detectable by phase changed-based satellite methods if the snow remains wet (i.e.,

contains liquid water) throughout the diurnal cycle, which can occur in the spring melt period, especially in deep snowpacks.

3.4 1:1 Daily Agreement Analysis

The first step of the analysis was to compare the satellite-detected snowmelt events and ground-based melt indicators at SRRW. In general, the goal was to understand how frequently both satellite and ground-based methods detect a melt event at the same time. To determine agreement between binary datasets (i.e., snowmelt detected, or not), I used a confusion matrix to calculate the true positive rate (or "sensitivity"; TPR), which defines how often a known positive event will be detected as positive by a predictor or proxy. A true positive (TP) occurs when both datasets detect a melt event, whereas a false negative (FN) occurs when melt is detected by the actual/true observation but is not detected by the proxy. True negative events, which occur when both datasets do not see melting, was not of interest in this study because we are primarily interested in the occurrence of melt events, not the lack thereof. Melt events are less frequent than days without melt, and therefore true negatives might inflate the agreement statistics. This type of analysis is typically performed on two binary datasets with the purpose of comparing true data to modeled or proxy data. In this study, neither satellite nor ground observations can be considered as "true" observations of a snowmelt event, because neither are direct observations of the presence of liquid water in the snow. Therefore, I perform the true positive rate calculation from two perspectives: assuming first 1) that the ground observation is the true observation, and a second time with 2) the assumption that the satellite is the true observation. Both analyses are important, depending on whether the goal is to determine how often satellite detected melt events are supported by ground data, versus how often ground-indicated melt events are detected by the satellite.

Equation 3 shows how the sensitivity was calculated when the ground-based melt events were treated as the "truth".

Equation 3: $Rate\ of\ True\ Positive\ (TPR) = \frac{TP}{FN+TP} = \frac{\#\ of\ days\ Ground\ and\ Satellite\ both\ detect\ melt}{Total\ \#\ of\ In-SItu\ melt\ events}$

The sensitivity was calculated a second time but instead using the total number of satellite detected melt events as the denominator. Both agreement analyses were repeated for all ground-based melt indicators at SRRW, as well as for snow depth and SWE derived melt indicators for the SNOTEL analysis.

For clarity, “sensitivity” and “rate of true positive” (TRP) herein refers the percentage of melt events that are detected by one melt indicator (“true”) that are also detected by another melt indicator (“proxy”). Since sensitivity is calculated both ways for each set of melt indicators, each calculation will be referred to by the indicator assumed to detect the “true” number of melt events. For example, the “SRRW 2022 Snow Depth Sensitivity” would refer to the number of matching melt events between the satellite and snow depth indicator divided by the total number of snow depth melt events, or “true melt events”.

For the Part 2 SNOTEL Analysis, three final agreement datasets were calculated: one that includes all sites with snow depth data; one that has all sites with SWE data; and a combined dataset that only includes sites with both SWE and snow depth data. Each of these datasets will from here on be referenced as the “Snow Depth Dataset”, the “SWE Dataset”, and the “Combined Dataset”.

3.5 Testing Correlations Between Snow Surface Characteristics and SNOTEL Analysis Agreements

For the regional SNOTEL analysis only, Spearman correlations were calculated for each of the 4 agreement datasets (snow depth vs. satellite, and SWE vs. satellite, with sensitivity calculated assuming each are the "true" melt events) to determine if the agreements varied by latitude, longitude, elevation, forest fraction, or average annual maximum SWE and snow depth. One-way Kruskal-Wallis tests were performed to determine if any of the snow classes had statistically significant differences in agreement. If so, a multiple comparisons test was then performed to determine which snow classes had significantly different agreements.

4. Results

4.1 SRRW Analysis

4.1.1 Overview of the 2022 and 2023 Winter Seasons

Time series of melts events detected by ground-based and satellite data for the winter of 2022 can be found in Figure 8. Timesteps when each individual melt indicator had NA values are depicted by shaded grey regions in their respective plots (Figure 8a-d). In 2022, snow depth measurements show a steady increase in snow through February, with some larger fluctuations in late February and early March indicative of potential midwinter melt and continuing snow accumulation. Steady melt seems to occur starting in mid-March, likely the melt output phase, although this cannot be confirmed without SWE measurements. The snowpack was completely melted by early April, although a few cm of snow accumulated afterwards in late April. Events from late April were not included in the analysis due to the small size of the snowpack that formed

(less than 5cm), which is below the 10cm height of the lowest temperature sensor. The satellite melt events almost exclusively occur during this second period of snow depth fluctuations, with the exception of one melt event occurring during a snow depth decrease in early December (Figure 8a). Both iButton temperature ladders also detected melt mostly during this period starting in mid-February and during snow depth decreases, except for some melts detected before a large snow depth increase (Figure 8b). This may also be due to the 20cm snow depth requirement for this melt indicator, as snow depth did not reach that depth until late January. Snow depth detected melt throughout the entire winter, as any decreases larger than 1cm were counted as a melt (Figure 8c). The HOBO temperature ladder also only detected melt events in the second half of the winter, although it is important to note that it did not start collecting data until January 20th, 2022. Some of the HOBO melt events occurred during large snow depth increases, contrary to all other melt indicators.

Time series of melts events detected by ground-based and satellite data for the winter of 2023 can be found in Figure 9. Timesteps when each individual melt indicator had NA values are depicted by shaded grey regions in their respective plots (Figure 9a-d). In 2023, the winter season started with a small early snowpack (< 20cm) in mid-November that completely melted in early December. Another snowpack quickly formed in mid-December but experienced another significant decrease in late December. After this period, the snowpack had a steadier accumulation through February, with larger snow depth fluctuations occurring throughout March. Snow depth steadily decreased starting in April and was completely gone by April 14th. One other significant event to note is the large snow depth decrease and immediate increase that occurred around December 19th. Based on further investigation and meteorological observations from the region, this is hypothesized to be a mixed precipitation event, with a potential rain-on-snow event causing

the drastic snow depth decrease followed by a switch to heavy snow accumulation accounting for the subsequent drastic snow depth increase depicted in Figure 9. It is also worth noting that 12-hour snow depth observations, such as used in 2022, would have likely not been able to detect such large variability, and highlights an important limitation of using data with a lower temporal resolution than 1 hour.

The satellite did detect a few melt events during the small November snowpack but did not detect any melt events in the snowpack that formed in December (Figure 9a). The rest of the satellite melt events occurred in February through April, and mostly coincided with falling or stagnant snow depths. The custom ladder melt events, depicted in purple points in Figure 9b, mostly occurred during a small snow depth decrease period in mid-February and during the melt-off period starting just after mid-March. A few melt events were also detected in December and January, with one event likely associated with the mixed precipitation event observed on December 19th. Similar to 2022, snow depth melt events were detected throughout the entire winter period (Figure 9c). IRT surface melt events were also detected throughout the entire winter, but mostly coincided with decreasing or stagnant snow depths (Figure 9d).

4.1.2 In-Situ Melt Indicator Comparisons

Because the in-situ melt indicators are all imperfect proxies for snowpack liquid water content, the sensitivity, or rate of true positive, was calculated between each of the SRRW in-situ melt indicators to determine how often they can mutually detect melt events. An example of the contingency table used for these agreements can be found in Figure 10, comparing iButton-detected melt events with HOBO-detected melt events. The yellow box indicates the number of melt events detected by both, blue is the total number of iButton melts, and the red is the total

number of HOBO melts. Table 2 shows a summary of the sensitivity values between each pair of indicators. In each case, the melt indicator listed in the column is assumed to be the "actual" or "true" total number of melt events, while the indicator in the row is the "predicted" melt events.

For the winter of 2022, in-situ melt indicators included snow depth (from camera images of a snow stake) and average snowpack temperature from 3 different temperature profiles. Snow depth had the overall lowest agreements with all other in-situ melt indicators, between 52% to 64%. The two iButton melt indicators had the highest agreements with each other, between 95.0% and 97.4%, which makes sense because these are the same temperature sensors that were simply mounted differently. The HOBO melt indicator also had high agreement with both iButton indicators, between 85.7% and 95.0%.

For the winter of 2023, snow depth from the SPA-2, surface temperature from the IRT, and average snowpack temperature from the custom thermistor temperature ladder were used as in-situ melt indicators. Agreements ranged from 42.4% between SD and custom ladder indicators to 76.9% between the Custom Ladder and IRT.

4.1.3 SRRW 2022 Agreements Between In-Situ and Satellite Melt Indicators

The agreements calculated between the in-situ melt indicators and the satellite melt indicator for both 2022 and 2023 are summarized in Table 3, which includes the total number of each melt event type, number of coincident events, and the sensitivity, assuming the in-situ and satellite-detected melt events as the "truth", respectively. In winter 2022, all four in-situ melt indicators detected at least three times more melts than the satellite algorithm. More in-situ melts resulted in much lower agreements when assuming those indicators were the "true" melts, and better agreements when assuming the satellite was the "truth". The total number of satellite melt

events differs due to occurrences of NAs in the datasets. The snow depth melt indicator detected 10 out of 13 satellite melt events and satellite detected 10 out of 51 snow depth melt events, or 76.9% and 19.6%, respectively. There were 34 total melt events from the HOBO temperature ladder, along with 11 satellite melts, and 8 detected by both. Therefore, the HOBO melt events matched with the satellite melt events for 72.7% of all satellite melts and for 23.5% of all HOBO melts. Both iButton melt indicators saw 31 total melt events and 11 satellite melts, with 8 and 9 matching events caught by iButton S and iButton F, respectively. Satellite agreement with iButton S was 72.7% (satellite as "truth") and 25.8% (iButton as "truth"), while iButton F agreements were the overall highest at 81.8% and 29.0%.

An Exact Binomial Test was also performed to determine if these agreements were likely a result of random chance rather than a true relationship between melt indicators. Using a p-value of 0.05, the alternative hypothesis states that the true probability of success (rate of true positive) is greater than the rate if melt events were randomly distributed throughout the winter. Using this test, all agreements between the satellite and in-situ melt indicators for the winter of 2022 were determined to be higher than what would be expected from random chance. In 2023, however, only the agreements between the IRT surface melt and the satellite melt showed significantly higher agreements than expected from random chance, while satellite agreements with the snow depth and custom temperature ladder melt indicators were not significantly higher.

4.1.4 SRRW 2023 Agreements Between In-Situ and Satellite Melt Indicators

In winter 2023, the number of in-situ melt events were again significantly higher than the number of satellite melt events for all analyses. The total number of snow depth melt events was 63 compared to 24 satellite melt events, with 11 events detected by both. As a result, they agreed

on 45.8% of total satellite melt events and 17.5% of total snow depth melt events. The IRT (surface temperature) detected the most melt events at 86 compared to 24 satellite melt events, with 23 melt events detected by both. This led to the overall highest agreements of the winter with 95.8% of satellite melt events detected by surface temperature and 25.8% of surface temperature melts also detected by the satellite. The final in-situ melt indicator for this year was average snowpack temperature from the custom temperature ladder, with 38 total melt events compared to 22 satellite melt events. Both indicators detected melt at the same time on 9 occasions, or 40.9% of satellite melts and 23.7% of the custom ladder melts.

4.2 SNOTEL Regional Analysis

4.2.1 Agreements Between In-Situ and Satellite Melt Indicators

The average sensitivities between the satellite and SNOTEL in-situ indicators across all sites are summarized in Table 4. This includes averages for the snow depth dataset, the SWE dataset, and the combined dataset that only include sites with both SWE and snow depth data. The number of sites in each dataset is provided in the second column for reference. Due to data limitations, some later analyses were only performed on the combined dataset. Melt events indicated by decreases in snow depth agreed with the satellite-detected melt events for 43% of all snow depth events, on average, and for 53.4% of all satellite melt events. Much lower average agreements were found using decreases in SWE as the snowmelt indicator, with SWE-indicated events agreeing with satellite-detected events for 39.7% of all SWE melt events, on average, and 27.8% of all satellite melt events. The distribution of agreements for all snow stations, and all sensitivity metrics, are summarized in boxplots in Figure 11. Red indicates analyses using the SWE

dataset, while blue indicates snow depth analyses. Both snow depth analyses have much smaller distributions of agreement among sites compared to both SWE analyses.

Exact binomial tests were again performed for all four agreement statistics for each of the 444 stations of the combined dataset with a p-value of 0.05. This test determined that 92% of sites had agreements between the satellite and snow depth melt indicators (for both $TPR_{Satellite}$ and TPR_{SD}) that were higher than expected due to random chance, while only 45% of sites had satellite/SWE agreements higher than expected from random chance.

Figure 12 summarizes the average seasonal distribution of melt events detected by each melt indicator for the snow depth dataset (Figure 12b, c), and the SWE dataset (Figure 12b, c). SWE melt events peak in May, while snow depth melt events peak in April, and satellite melt events from both datasets peak much earlier in March. Snow depth also indicates more melt events throughout the year compared to the satellite and SWE.

4.2.2 Correlations

The next step of the SNOTEL regional analysis was to investigate spatial patterns of agreement across different sites, as well as land characteristics of the snow stations and their surrounding satellite pixels. Figure 13 shows a map of sensitivity of each snow station for each analysis. A notable pattern shown by these maps is a group of sites with generally high agreement located in the Sierra Nevada Mountain Range. This trend is most visible in both snow depth analyses and is also somewhat visible in the SWE datasets. Figure 14 shows violin-boxplot comparisons of agreements at all sites vs only the Sierra Nevada sites for the SD analysis (a) and the SWE analysis (b). Unlike the snow depth dataset, the SWE dataset contained sites outside of the SNOTEL network, including 29 sites in the Sierra Nevada Mountains, allowing for more data

in the SWE comparison. Kruskal-Wallis tests were also performed with a p-value of 0.05 and found all sensitivities were significantly higher in the Sierra sites compared to the rest of the dataset.

Different site characteristics were then tested for correlation with each agreement metric using a Pearson correlation test, with the results shown in Figure 15. Due to a large sample size of 444 sites, most correlations were found to be statistically significant at a significance level of 0.05, even with very low correlations. Correlations that are not statistically significant are marked in grey Figure 15. Elevation appears to have the highest correlation with most agreement metrics, including 0.5 correlation with the snow depth-satellite melt agreement (assuming satellite events are the "truth"). The correlations are also all positive, suggesting that higher elevation sites have higher agreement. The snow depth-satellite melt agreements also seem to have the highest correlations for most variables tested. Latitude has similarly high correlations with all agreement metrics but are instead all negative. This suggests that the satellite and SNOTEL melt indicators agree better at sites located farther south. Elevation and latitude of snow sites has a correlation of -0.8, indicating that higher agreement may only be tangentially associated with one (or both) of these variables. Longitude was also tested but found much weaker positive correlations between 0.2 and 0.3. The next variable tested for correlations with agreement was “Max SD”, or the average of the annual maximum snow depth recorded at each site across all years. The most significant and largest correlation by far was with the SD-satellite agreement, with a correlation of 0.4. This suggests that the snow depth indicator can detect a higher percentage of satellite-detected melts at sites with deeper snowpack. The same statistic but for max SWE was also tested, resulting in correlations of 0.3 for the satellite (SD) agreements and -0.4 for the SWE agreements. This promotes the previous suggestion of snow depth detecting more satellite melt events at sites with

larger snowpack, but it also suggests that the satellite can better detect SWE melt events at sites with smaller snowpacks. The percent tree cover at each snow station was also tested, resulting in negative but generally low correlations below -0.2. If correlations were stronger, this would have indicated that sites with less tree cover have better agreement. The tree cover percentage over the entire AMSR-E pixel was also tested, with a negative correlation of -0.2 with agreements in the SD dataset. This may suggest that the satellite can better detect snow depth melt events when the satellite pixel has overall less vegetation/tree cover.

The last analysis of differences in satellite vs. in-situ agreement across SNOTEL sites was by snow class (see section 3.5). Only the snow classes of Tundra, Boreal Forest, Montane Forest, Maritime, and Prairie were tested due to a lack of sites located in regions assigned to the Ephemeral snow class. Using a Kruskal-Wallis test, it was determined that only the satellite-snow depth agreement metrics had any statistically significant differences between the means of any of the snow class groups. A Dunn's test indicated that for the snow depth sensitivity assuming snow depth as "true", only the Boreal Forest and Montane Forest groups have significantly different medians. For the snow depth sensitivity assuming satellite melt as "true", only the Boreal Forest and Prairie groups have significantly different medians.

5. Discussion

5.1 Limitations of Data

The results of these analyses are dependent on the accuracy and representativeness of the input data. Biases and uncertainty in the data can affect the results, therefore is it necessary to discuss the limitations of the data used.

5.1.1 In-Situ Data

The use of point-scale data for understanding temporal trends of a snowpack comes with inherent limitations due to the high spatial variability of snow, especially in mountainous or heterogeneous landscapes (Meromy et al., 2013; Sexstone et al., 2016; Watson et al., 2006). Locations less than 1 km apart can have significant differences in snowpack properties, including snow depth and temperature, due to atmospheric and land surface conditions.

In-situ data were collected firsthand for the SRRW analyses, allowing for better knowledge of the errors and uncertainty associated with the data collection. For 2022, the snow depth from the SPA-2 was unreliable, and therefore snow depth was determined using visual identification of snow height from 12-hour camera images of the snow stake. Besides inherent human error and uncertainty in determining snow depth, a fair number of observations were not available due to poor visibility in photographs due to precipitation accumulation on the lens or sunlight reflectivity on the snowpack. There also may be error in the HOBO temperature ladder data during this year as it was installed on January 20th, after the snowpack had already formed. The snowpack was significantly disturbed during installation and potentially altered temperatures within the snowpack throughout the remainder of the winter. The field site was also visited on February 7th of 2023 for instrument maintenance, and while care was taken not to disturb the snow directly around instrumentation, it is possible that disturbances did occur. There is also error and uncertainty associated with each of the temperature ladders due to the sensitivities of the sensors to solar radiation, as well as from preferential melting around the ladders from heat conductance of the structure. It is important to note that only two years of data were included in this study, which may not be representative of typical conditions at this location. Future data collection at this site and potential surrounding locations can help improve and confirm these results.

There are also significant limitations associated with the SNOTEL and associated snow network data. One of the more significant limitations of the SNOTEL network specifically is the lack of spatial distribution and diversity among stations. The original purpose of SNOTEL was to monitor mountain snow conditions in the Western US for water resource monitoring. Therefore, it's not surprising that most sites are located in regions that are important for that purpose (Fleming et al., 2023; Heldmyer et al., 2021; Schaefer, 2000). The downside, however, is the systematic bias towards specific elevations and land cover types within the SNOTEL network, as seen by the proportions of snow classifications among SNOTEL sites in Figure 6. Most sites are also located in clearings, therefore muddying attempts at understanding potential correlations between vegetation cover and snowpack dynamics. There is also a lack of diversity in types of data collected at each station. While SWE and snow depth measurements were the focus for hydrologic snow monitoring, there has been an increasing need for different types of snowpack measurements, such as snow temperature and liquid water content (LWC).

A practical limitation of SNOTEL data relevant to this study is the fact that quality-controlled datasets are only published with daily average data for both SWE and snow depth, despite data collection at a shorter timestep. Daily observations are insufficient to understand the dynamics of snowpack melt due to diurnal fluctuations. Within 24 hours, many different processes and events can take place which can significantly alter the physical state of the snowpack including melt, refreeze, new snowfall, and rain on snow events.

5.1.1 Satellite Data

There are many limitations of the satellite data used in this study, including the large spatial resolution of 25km. Heterogeneity of the land surface within the boundaries of a 25km pixel have

the potential to obscure melt signals from colder or higher elevation regions located within the pixel. This limitation is enhanced when using point-based ground data for validation, as conditions at one snow station are likely not representative of a 25km region. It is also very likely that in-situ melt indicators can respond to local or small-scale melt events, which may not occur throughout the entire pixel region, and therefore the satellite may not be able to detect it. This is especially true for mountainous regions with steep elevation changes associated with extreme differences in weather conditions. Snowmelt distribution is also heavily influenced by topographic variability and its effects on solar radiation (Cline, 1997; Marks & Dozier, 1992; Vuyovich et al., 2017). More generally, a lack of snow cover over a majority of a pixel may also cause bias in the brightness temperature, as bare ground vs snow can have significant influences on passive microwave radiation (Chang et al., 1996; Mätzler, 1994) and obscure possible melt signals. Studies have also suggested that microwave signals may not fully penetrate through moderate to dense vegetation canopies (Chang et al., 1996; Foster et al., 1991; Lund et al., 2022).

An additional limitation of the satellite data is the saturation of the microwave signal in deeper snowpacks. Studies have estimated that at 37GHz frequency, snow depths greater than 0.8-1 m cause microwave emissions to be "saturated" and therefore undetectable by the satellite (Chang et al., 1976; Dong et al., 2005; Foster et al., 2005). While the ΔT_b-ΔT_a method may correct for the influence of air temperature on microwave signals, it is not able to correct for potential rapid changes in snowpack properties such as snow texture and grain size (Chang et al., 1976; Foster et al., 2005; Sturm et al., 1995). Change-based satellite melt detection methods cannot detect consistently wet snow (Tuttle & Jacobs, 2019), only phase changes. This study also does not take into account rain-on-snow events, although some PMW rain-on-snow detection methods rely on

similar wet snow sensitivities, suggesting that they may produce similar brightness temperature signals (Dolant et al., 2016; Grenfell & Putkonen, 2008).

5.2 In-Situ Snowmelt Indicators

As supported by results from both the SRRW and SNOTEL analyses, decreases in snow depth is not an ideal indicator of melting snow. While melting snow can cause decreases in snow depth due to densification or loss of snow mass, there are also many other processes that cause snow depth to decrease that are not indicative of melt. These other factors could explain the large number of potential melt events inferred from snow depth in comparison to the number of melt events detected by the satellite. Besides melting, snow depth can decrease due to compaction. This is very common after fresh snowfall, as snow grains initially settle and pack together due to gravity (Pomeroy et al., 1998). Compaction also occurs throughout the winter season due to a combination of gravity and pressure of lower layers, especially in deeper snowpacks. Decreases in snow depth can also be caused by removal of snow due to sublimation, wind redistribution, and rarely, avalanches (Hiemstra et al., 2006; Marks & Dozier, 1992). Due to these common processes affecting snow depth decreases and the potential for false melt identifications, snow depth is not an ideal indicator for snow melt events. It is, however, one of the few variables collected by SNOTEL that contain some information potentially related to snowmelt and snow liquid water content.

Although SWE is a proven useful snowmelt indicator (Serreze et al., 1999), SWE decreases had much worse overall agreements with the satellite melt detection method compared to snow depth. The main limitation of this metric is that it can only be used to detect hydrologically significant melt events, where water is leaving the snowpack. PMW satellite instruments are

sensitive to the presence of liquid water in the snowpack, which may occur due to snowmelt and subsequent refreezing of the liquid water without a loss of water from the snowpack. While processes such as compaction may not decrease SWE, physical displacement of snow due to sublimation, wind redistribution, and the occasional avalanche may lead to false melt event detection using this indicator.

Based on the results from the SRRW analysis, average snowpack temperature is a decent indicator for detecting snow melt events. Theoretically, as a snowpack approaches 0°C, melting is more likely to occur with minimal energy input into the system. In reality, however, melting can occur nonuniformly throughout the snowpack, with some layers not yet reaching 0°C. One of the most common examples of this is solar radiation causing surface melting at the top of the snowpack, while deeper layers may still be well below 0°C. The practicality of this method is also dependent on the vertical resolution of these temperature measurements, as well as the depth of the snowpack. Our method used the average temperature of the snowpack as detected by temperature sensors located every 10cm, while excluding sensors less than 10cm from the surface due to welling around the instruments. Our method began measurements at 10cm above the ground and excluded sensors less than 10cm from the top of the snow, automatically excluding any melt detection in snowpacks less than 20cm. In the future, these data could be used for different melt indicators, such as detecting melt events within specific layers of the snowpack (i.e., bottom, middle, surface).

Overall, data from the SRRW analysis supports the hypothesis and previous studies that the surface temperature of the snowpack (as measured by the IRT) and subsequent surface melt events most closely resemble the processes detected by this satellite melt detection algorithm. In 2023, 23 of the 24 satellite detected melt events were detected by the surface temperature indicator,

resulting in a 95.8% agreement. This indicates that almost all the satellite detected melt events were corroborated by surface temperatures at or above the melting point of snow. This also supports the idea that passive microwave satellites at 36GHz is sensitive to snowmelt on the surface of the snowpack. While surface temperature may not be as important for detecting hydrologically significant melt events, our results show that it is a viable melt detection indicator for ground truthing passive microwave satellite melt detection methods. However, this indicator also produced many false positives (i.e., days when the daytime snow temperature was near 0˚C but the satellite did not detect melting). It is unclear if this is due to the location of the IRT in a clearing, while much of the surrounding satellite pixel consists of forest. On the other hand, the snow surface temperature may frequently reach close to 0˚C without producing snowmelt.

The most ideal observations for detecting wet or melting snow are liquid water content observations, as they directly measure the amount of liquid water present in the snow and can track increases indicative of true snow melt. LWC are also theoretically ideal for ground truthing of PMW melt detection algorithms due to findings from (Mätzler, 1987; Stiles & Ulaby, 1980) which state that PMW brightness temperature observations are directly correlated with the dielectric constant of a snowpack. Since frozen snow and liquid water have drastically different dielectric constants, the proportion of the two within a snowpack should have a strong influence on the brightness temperature of a land surface detected by PMW satellite, along with air temperature (Equation 1). Therefore, having direct measurements of liquid water content in a snowpack would allow for more accurate analyses of the effect of liquid water on melt detection algorithms. Unfortunately, LWC measurements are very rare due to the complicated and expensive nature of the instruments needed for non-destructive continuous monitoring, as learned from the ongoing effort using the SPA-2 at SRRW.

5.3 PMW Satellite DAV Melt Detection Method

The results at the Vermont study site (SRRW) demonstrate that while this PMW melt detection method is not able to detect all melt events that may occur at a snow station, certain ground melt indicators verify that a large portion of satellite detected melt events can be corroborated by ground data. This is expected due to the limitations of comparing large-scale observations that encompass 25km with point data, especially given the high spatial variability of snowmelt. Specifically, 23 out of 24, or 95.8%, of the satellite-detected melt events during 2023 were verified by the IRT ground melt indicators (i.e., snow surface temperature). The satellite also showed consistent melt detection during the beginning of in-situ-detected multi-day melt periods during the winter of 2022, which is consistent with the detection of phase changes rather than continuously wet snow, as expected.

In the SRRW site analysis, the satellite melt indicator was able to detect 77% of snow depth-detected melt events in the winter of 2022, but only 46% in the winter of 2023. This may be attributable to the different number of melt events detected by the satellite in those years (13 and 24, respectively), or to the difference in snow depth measurement techniques each year (manual vs snow depth sensor, respectively). For the SNOTEL regional analysis, the snow depth melt indicator was able to detect an average of 53% of satellite-detected melt events, which matches ranges of the 2023 SRRW. There are also large differences the sensitivities calculated for total satellite melt events detected by snow depth (satellite as “true”), as the SNOTEL analysis found a much higher average sensitivity of 43% compared to the SRRW analyses of 17% and 20% for 2022 and 2023, respectively. This may be due to the use of maximum daily air temperature to restrict snow depth melt events at SNOTEL sites, which was not able to be done for SRRW, or from the use of 12-hourly measurements at SRRW and daily snow depth measurements at

SNOTEL stations. It is also important to note that while SRRW is classified as being a montane forest snow class, similar to the majority of sites in the SNOTEL study, there may be other factors not considered in this classification that can affect snowpack characteristics, specifically between West and Eastern snowpacks.

Low overall agreements between the satellite and SWE/snow depth indicate fundamental differences in how each indicator identifies melt. While more common at individual snow measurement sites and easier to measure than LWC, large snow station networks such as SNOTEL do not include instrumentation to collect snow surface temperature. This gap in snow radiation and melt data within snow monitoring networks hinders the ability to perform large-scale analyses of satellite melt detection methods. Without better melt proxies available across a wide range of snow stations, the usefulness of findings from further regional analyses of this PMW melt detection method may be limited. Although significantly better agreements between the satellite and ground data were observed in all analyses for stations located within the Sierra Nevada Mountain Range, without ground-based observations that are more reflective of snow liquid water content it is hard to determine if these agreements are statistically meaningful or if there are unique characteristics in the snowpack in this mountain range that allow this satellite method to perform better.

Positive correlations between agreements and elevation suggest that this melt detection method performs better at higher elevations. This may be due to sites at higher elevations having longer snow seasons, allowing for better calibration of the ΔT_b-ΔT_a relationship at these sites. Negative correlations with latitude suggest that there may be other factors causing higher agreements at sites in lower latitudes of the Western US, although this needs to be investigated further. Although correlations were overall low with site and pixel tree cover, all significant relationships with agreement were found to be negative. This corresponds with previous studies,

which found that microwave signals were not able to fully penetrate vegetation canopies (Chang et al., 1996; Foster et al., 2005; Lund et al., 2022).

Due to the low agreement and differences in seasonality between the satellite and SWE melt detection indicators (Figure 12), it can be concluded that this modified ΔT_b-ΔT_a melt detection method is not appropriate for detecting hydrologically significant melt events. Hydrologically significant events occur when liquid water is released from the snowpack into the surrounding environment and is often associated with consecutive days of high liquid water content in the snowpack (Johnson et al., 2020). The ΔT_b-ΔT_a method relies on detecting physical changes in the snowpack from dry to wet snow, and therefore continuously wet snow will not be detected. This is also supported by the relatively lower agreement between the satellite-detected melt events and the isothermal melt indicators in the SRRW study in 2023, compared to the agreement between the satellite and the IRT snow surface melt indicator. I find that the satellite melt detection method is instead best suited to detect surficial and/or midwinter melt events, as well as confirming the onset of hydrologically significant melt events. This method may also be useful for providing information about the energy balance of a snowpack, such as when the snowpack is warming up, along with being used for energy inputs for snowpack modeling in remote regions (Langlois et al., 2012). This method could also be useful for the assimilation of PMW derived snow depth and SWE data into models (J. Ramage & Semmens, 2012), as it can help determine when the snowpack is wet and therefore the PMW data are not reliable for inferring snow depth or SWE (Frei et al., 2012).

Results from this study are well aligned with those from previously literature. Johnson et al. (2020) used similar snow depth melt proxy techniques to validate a standard threshold-based melt detection algorithm with the same AMSR-E 25km 37GHz frequency PMW dataset. Their

DAV method was able to detect 46% of all melt events at three study sites in Colorado for one winter season. This matches very closely with results from my SNOTEL analysis, which showed an average TPR of 43% for 481 study sites over 9 years. They also similarly conclude that diurnal PMW melt detection methods are better suited for detecting mid-winter surface melt and refreeze events, and that snow depth and SWE data is not sufficient for true validation of these satellite methods. Johnson also found that the higher resolution AMSR-E data product increased the overall TPR to 78%. High resolution downscaled PMW observations are not included in this thesis as similarly processed data is not yet available for the AMSR2 satellite but could be investigated when data becomes available. Due to the novel nature of this research, there are few relevant studies with similar analyses and techniques that allow for direct comparison of quantitative results. Validation efforts of similar DAV methods have achieved comparable quantitative results. Ramage & Isacks (2002) used air temperature and stream discharge data to validate their original DAV method on the glaciers of Alaska and Northwestern Canada. They found significant relationships between DAV and stream discharge, suggesting their method was able to capture real transitions in the melt cycle rather than full hydrologic melt events. Li et al. (2012) evaluated AMSR-E DAV melt onset days using snow pillow SWE data in the Sierra Nevada Mountains. They demonstrated that PMW observations do contain valuable information about snowpack melt cycles in mountainous terrain, and they also found that diurnal air temperature variations were highly correlated with diurnal brightness temperature variations (DAV). In this context, Tuttle & Jacobs (2019)'s ΔT_b-ΔT_a method was the next logical step in improving snow melt extraction from PMW observations.

6. Conclusions

Detailed and continuous in-situ snowpack observations from Sleeper's River Research Watershed provide a unique opportunity to investigate snowmelt detection methods using passive microwave brightness temperature observations. Surface temperature of the snowpack was the best indicator of melting snow, as defined by the transition of frozen water from a solid to a liquid state in the topmost layer of the snowpack. However, all ground-based melt indicators also resulted in high false positive rates. Hydrologically significant melt events, best captured by observations of SWE and internal snowpack temperature, are not well distinguished by the modified ΔT_b-ΔT_a PMW satellite melt detection method, with the exception of the initial transitional period as described by Ramage & Isacks (2002). While the dense networks of snow monitoring stations throughout the western US and Canada can provide vital snow depth, SWE, and meteorological data for runoff and water availability forecasts, current SNOTEL observations do not provide direct observations that would allow for the advanced prediction of snowmelt. The addition of instrumentation to measure snow internal and/or surface temperature will help improve validation efforts of PMW melt detection methods, which could aid in better snowmelt forecast modeling.

Figures

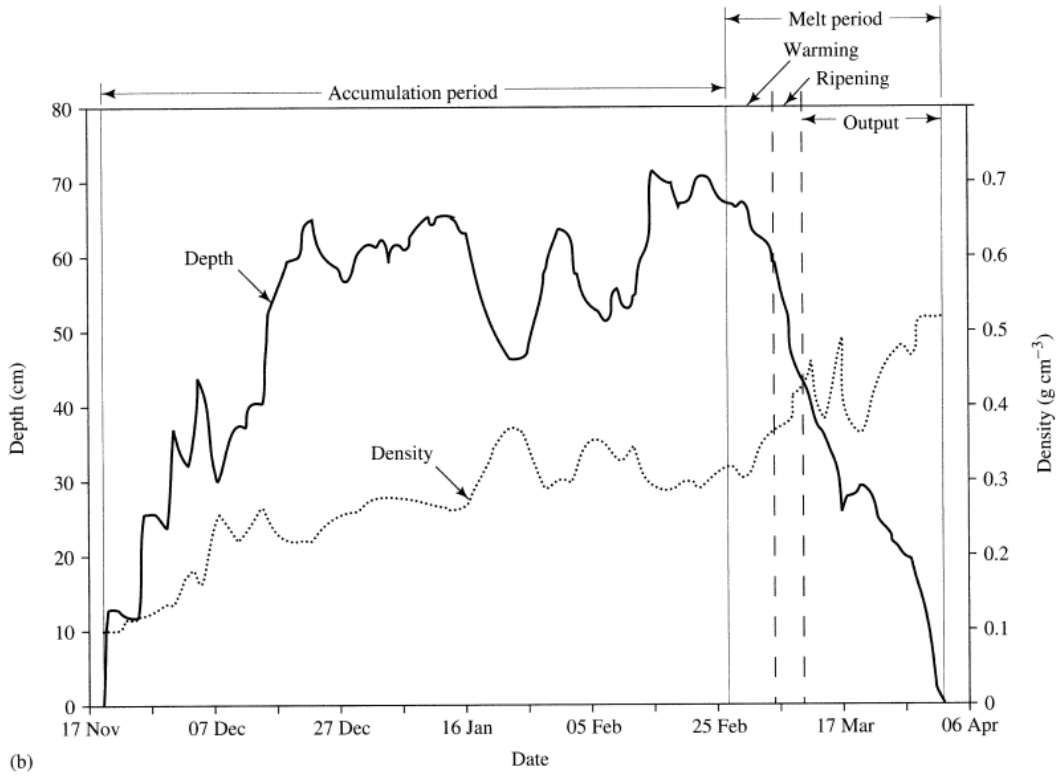

Figure 1: Timeseries of snow depth and snow density data at Sleeper's River Research Watershed, 1972-1973, showing the accumulation period and the different stages of ablation (melt) for the snowpack. Figure from Dingman (2014).

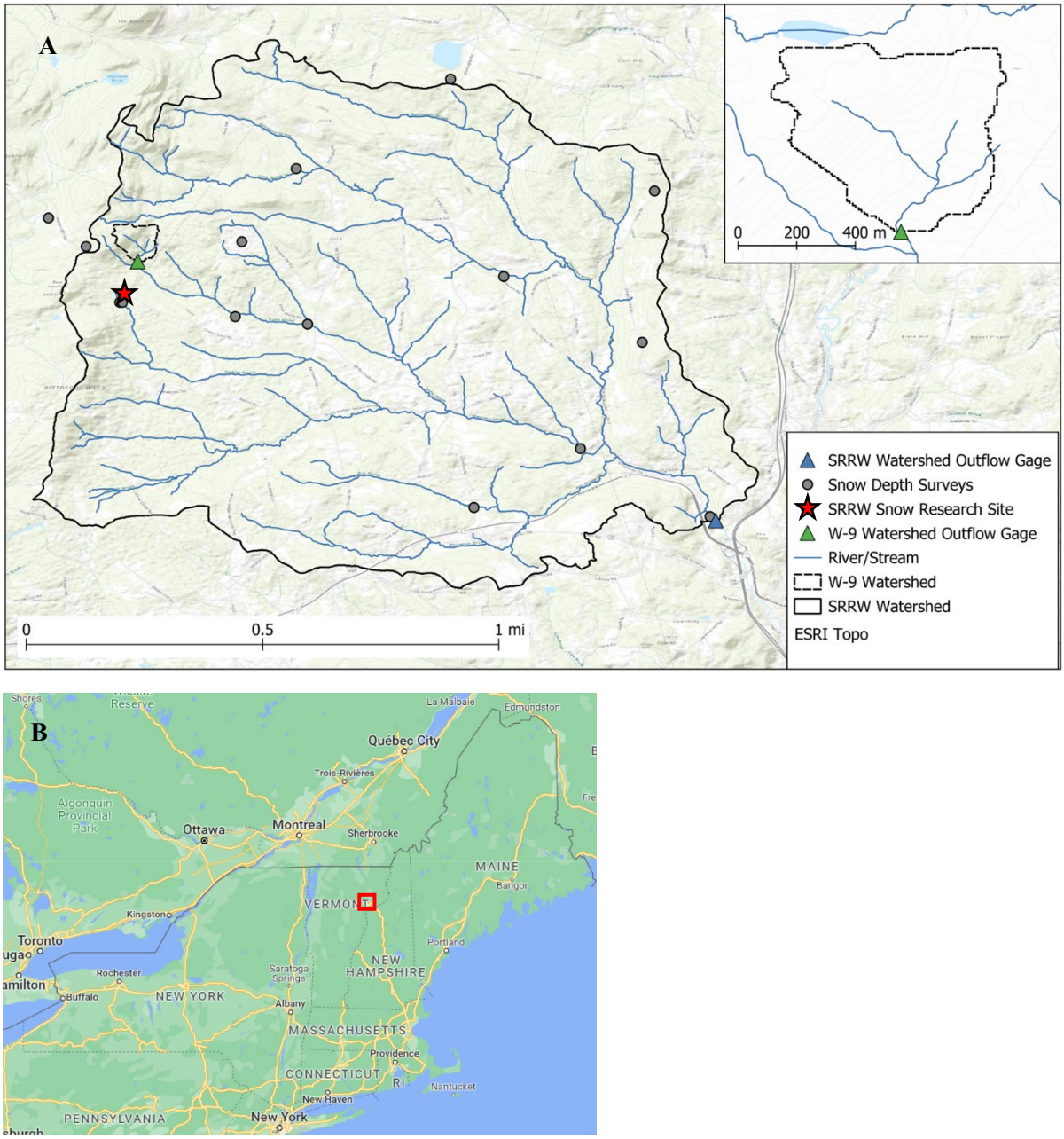

Figure 2: a) Map of Sleeper's River Research Watershed and instrumentation locations (red star). Blue lines indicate river/streams. Solid line represents boundary of watershed. Grey points are locations of USGS weekly SWE and snow depth sampling locations. Triangles indicate locations of stream gauges. **b)** Regional map of study site, outlined in red (Google Maps, 2023).

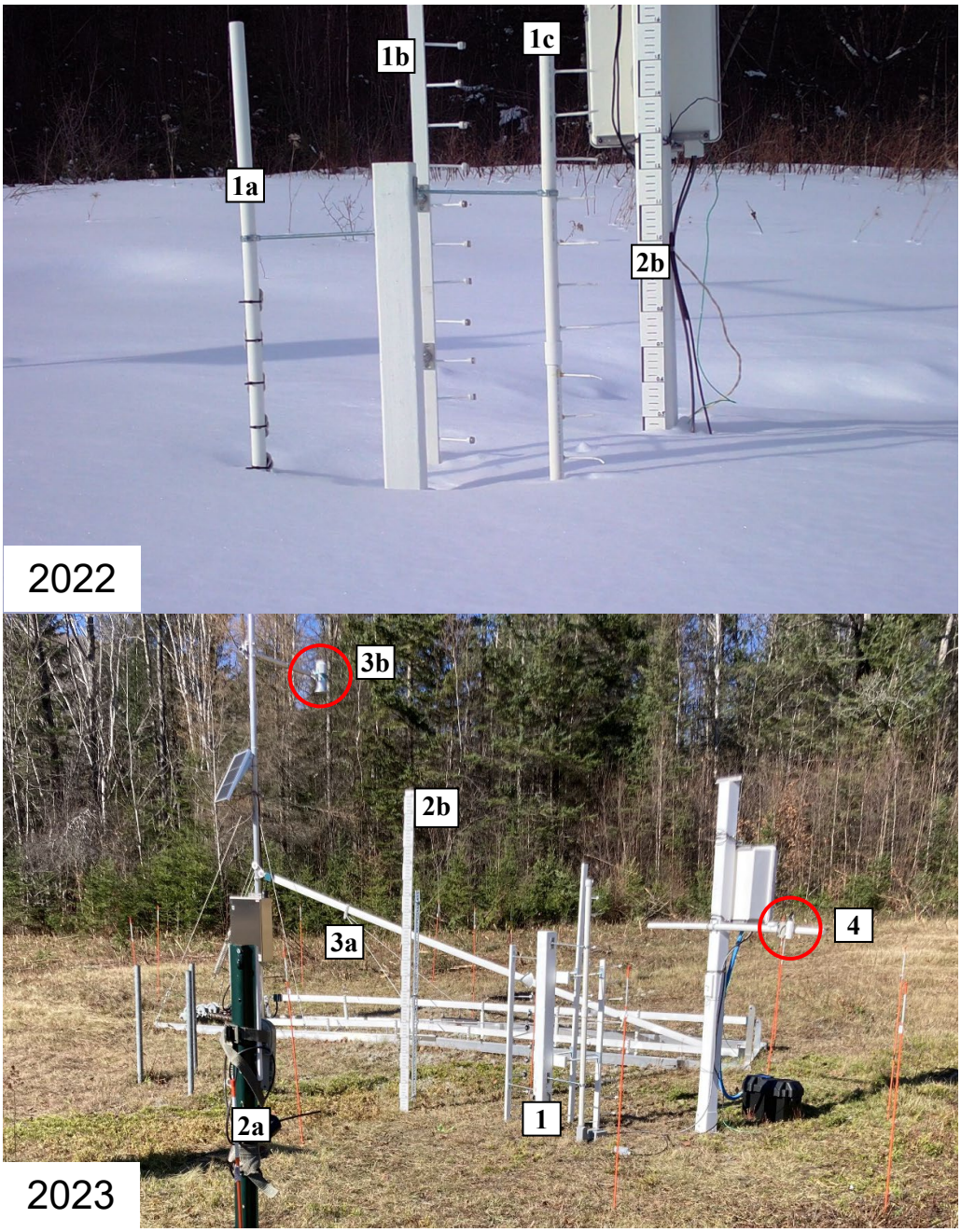

Figure 3: Sleeper's River Research Watershed Tuttle research instruments for water years 2022 and 2023. **1)** Vertical snow temperature ladders using: **1a)** HOBO MX2201temperature data loggers, **1b)** iButton temperature sensors mounted on poles facing east (iButton S) and another set mounted directly on the stake facing north (iButton F), and **1c)** custom thermistor sensors (from Eric Kelsey, Plymouth State). **2a)** Wingscapes Timelapse Pro camera and **2b)** snow depth stake to record photographs of snow depth every hour. **3)** Snow Pack Analyzer-2 (SPA-2) with **a)** dielectric measurement bands and **b)** ultrasonic snow depth sensor. **4)** Apogee Infrared Radiometer (IRT)

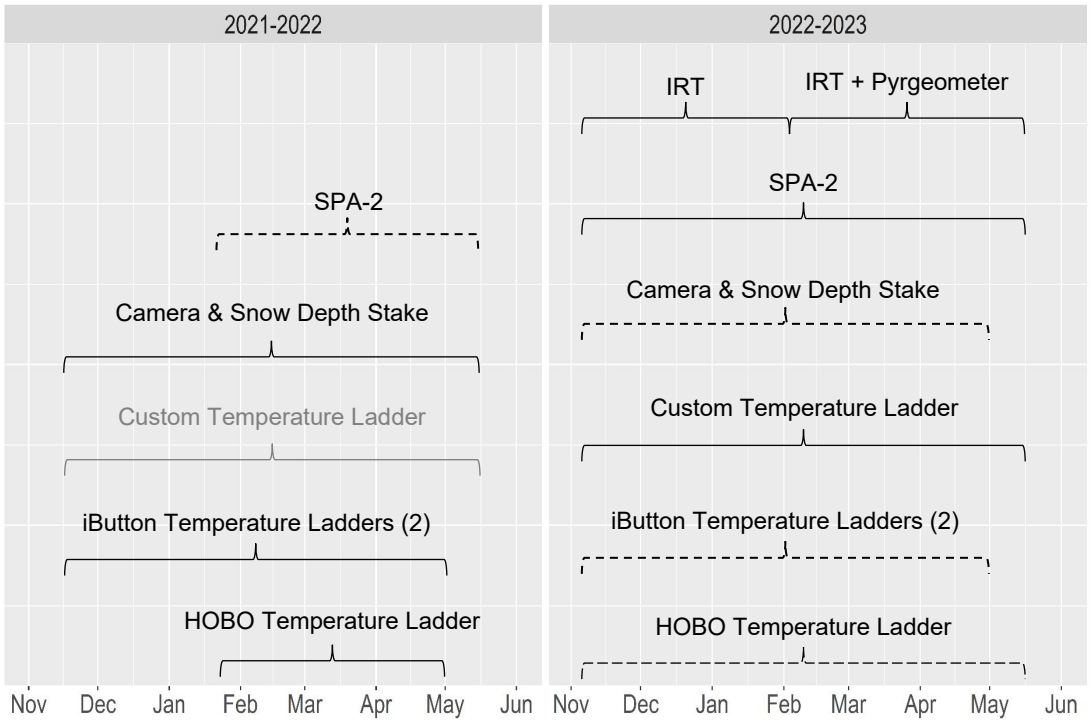

Figure 4: SRRW instrument data availability. Solid lines indicate data included in analysis, dashed lines indicate data collected but not included, grey indicates no data collected.

Table 1: Summary of all melt indicators used for each analysis for SRRW 2022, SRRW 2023, and SNOTEL 2002-2011.

Study	Melt Indicator	Measurement Type	Instrument	Units	Spatial Resolution	Temporal Resolution
SRRW 2022	*Snow Depth*	Snow Depth	Snow Stake and Wingscapes Timelapse Camera (manual)	cm	Point	1 hour
	HOBO	Snowpack Temperature Profile	HOBO MX2201 Water Temperature Data Loggers	°C	Point	10 minutes
	iButton F	Snowpack Temperature Profile	iButton DS1922L Temperature Data Loggers	°C	Point	1 hour
	iButton S	Snowpack Temperature Profile	iButton DS1922L Temperature Data Loggers	°C	Point	1 hour
	Satellite	ΔTb-ΔTa	AMSR2	K	25x25 km	12 hours
SRRW 2023	*Snow Depth*	Snow Depth	SPA-2 Ultrasonic Sensor	cm	Point	10 minutes
	Custom Ladder	Snowpack Temperature Profile	Campbell Scientific Thermistor Temperature Sensors	°C	Point	10 minutes
	IRT	Surface Temperature & Downwelling Infrared Radiation Correction	Infrared Radiometer Sensor (IRT) & Pyrgeometer	°C	Point	10 minutes
	Satellite	ΔTb-ΔTa	AMSR2	K	25x25 km	12 hours
SNOTEL (2002-2011)	*Snow Depth*	Snow Depth	Ultrasonic Sensor	cm	Point	Daily
	SWE	Snow Water Equivalent	Snow Pillow	cm	Point	Daily
	Satellite	ΔTb-ΔTa	AMSR-E	K	25x25 km	12 hours

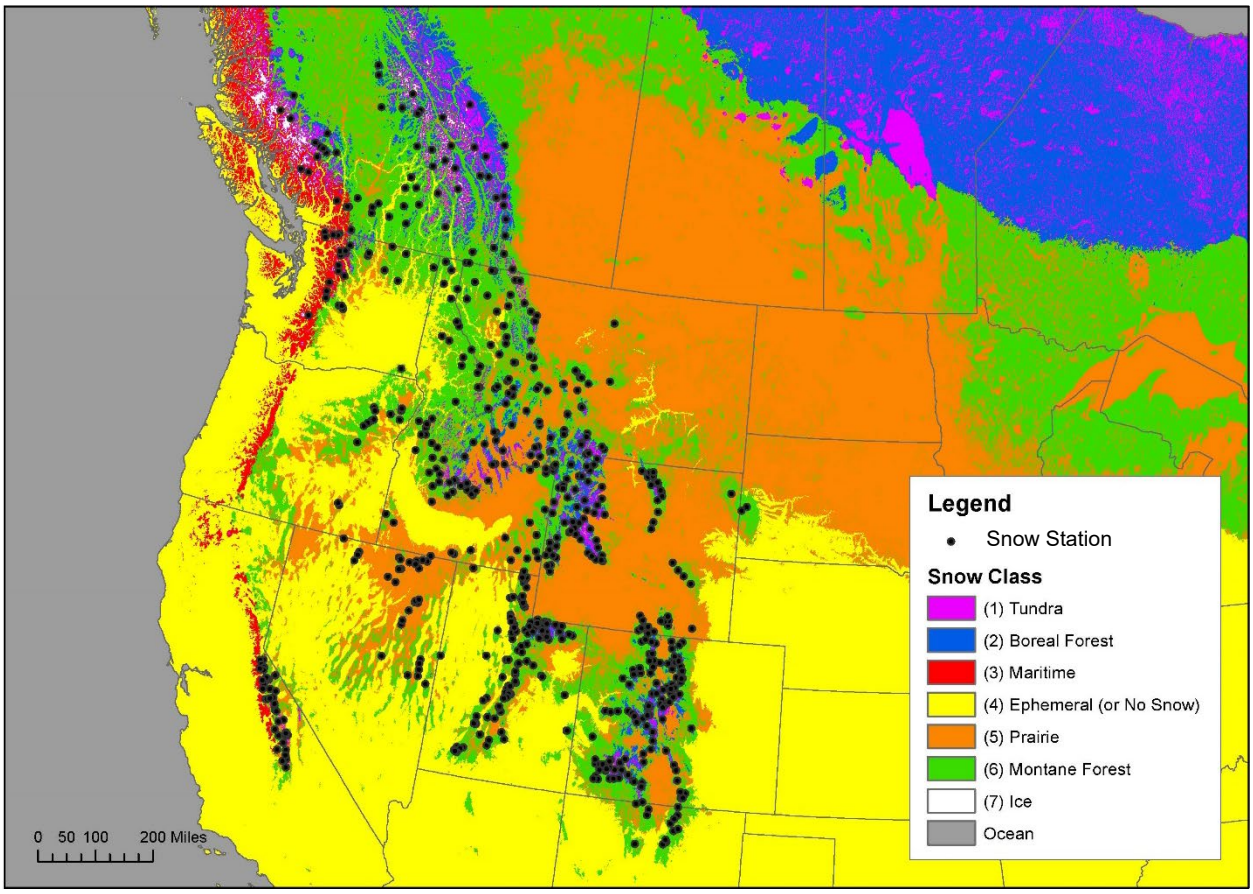

Figure 5: Map of snow climate classes (Sturm & Liston, 2021) and ground-based snow measurement stations (Musselman et al., 2021) across the western U.S. and Canada. The snow climate classes represent variations in snowpack characteristics (such as density, layers, crystal structure, etc.) derived using three climatic variables: wind speed, precipitation, and air temperature. For example, the Tundra snow class (purple) has characteristically dry snow that is heavily blown by wind and little to no melt features. The Ephemeral snow class (yellow), conversely, describes a thin, wet snowpack that frequently melts and reforms throughout the winter.

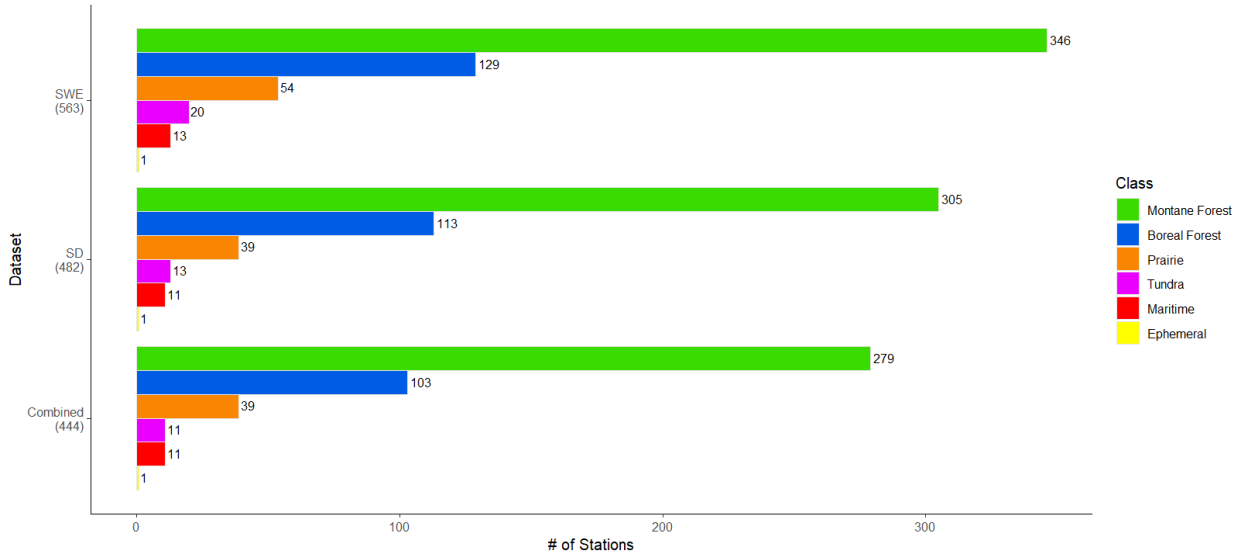

Figure 6: Distribution of snow classifications for study sites within the SWE dataset, the Snow Depth dataset, and the combined dataset, using the updated high-resolution seasonal snow classification map (Sturm & Liston, 2021). Total number of stations in each dataset are also provided on the y-axis. Only stations with non-NA agreements were included.

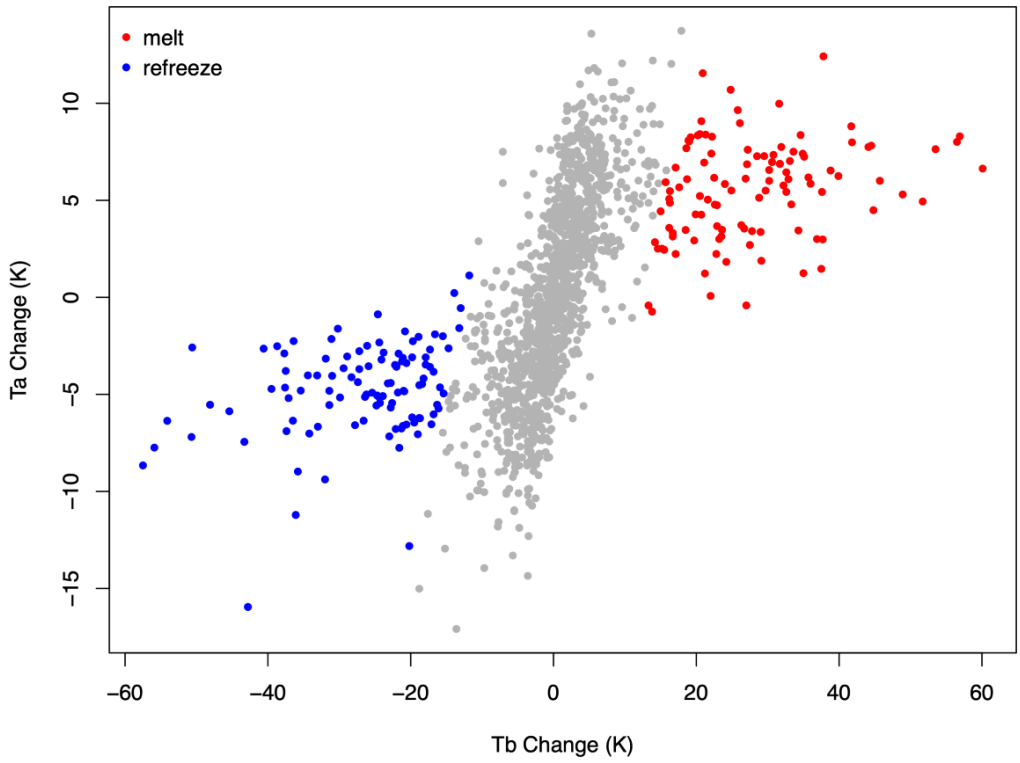

Figure 7: Diurnal change in air temperature (y-axis) plotted against diurnal change in brightness temperature (x-axis) for snow covered periods for an AMSR-E pixel in the Northern Great Plains, USA, 2002-2011. The grey cluster of points represents was found to have a linear relationship between change in air temperature and change in brightness temperature over completely frozen snow for this location using modal linear regression. Melt (red) and refreeze events (blue) were identified as significant deviations from the ΔT_b-ΔT_a line using k-means clustering. (Updated figure from Tuttle et al, 2019).

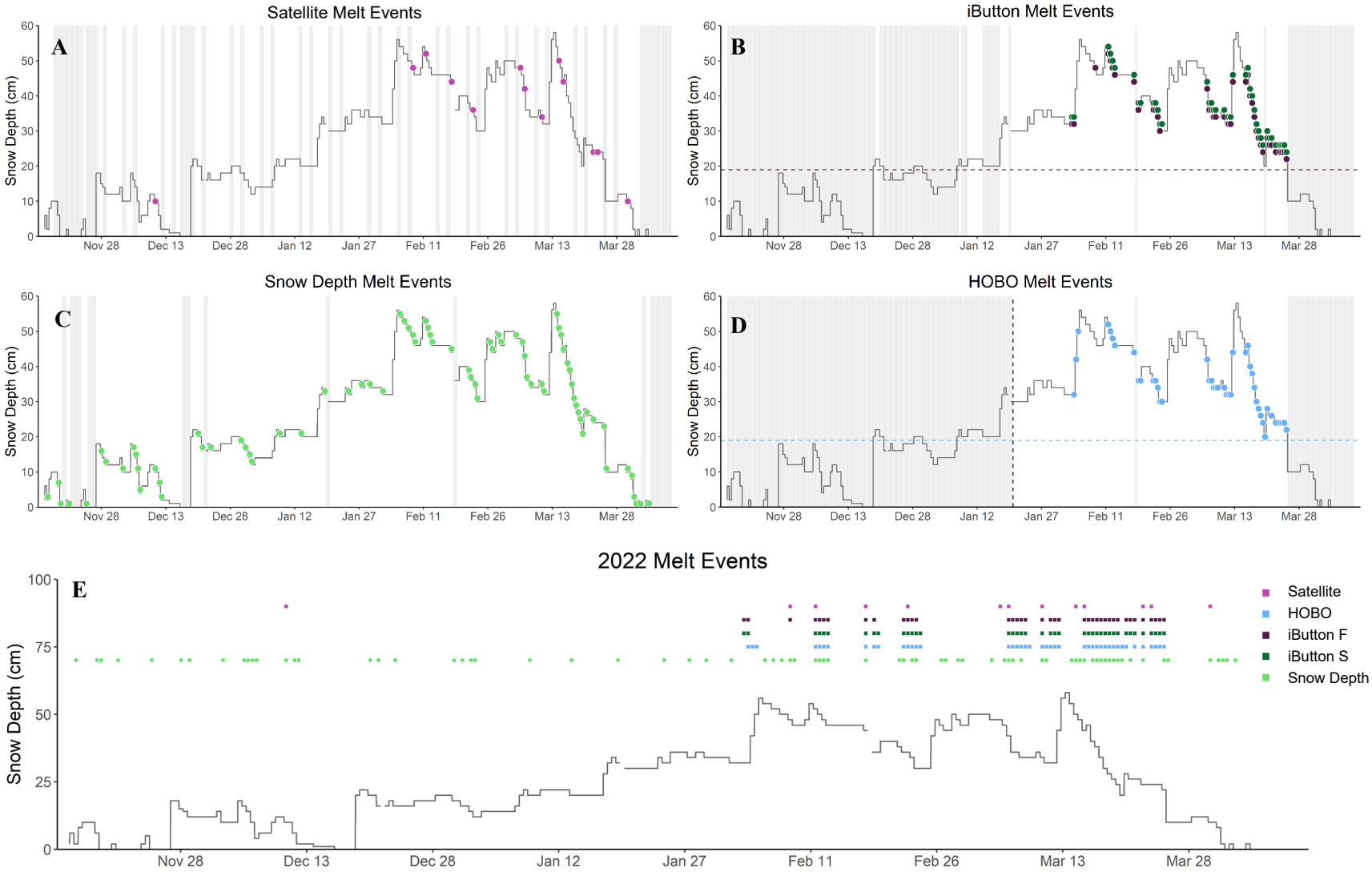
Satellite Melt Events
A
iButton Melt Events
B
Snow Depth Melt Events
C
HOBO Melt Events
D
Snow Depth (cm)
Nov 28
Dec 13
Dec 28
Jan 12
Jan 27
Feb 11
Feb 26
Mar 13
Mar 28
2022 Melt Events
E
Satellite
HOBO
iButton F
iButton S
Snow Depth

Figure 8: Timeseries of 12-hour snow depth measurements at SRRW for the 2021-2022 winter with **a)** satellite, **b)** iButton, **c)** snow depth, and **d)** HOBO melt events. Horizontal dashed lines in **b)** and **d)** indicate 20cm snow depth thresholds necessary for temperature ladder melt detection (iButton and HOBO). **b)** includes both iButton F and iButton S melt events as they are almost identical. Vertical dashed line in **d)** indicates time when the HOBO temperature ladder was installed midwinter on January 20th, 2022. Grey shaded time periods on **a)** – **d)** indicate times when each respective melt indicator is NA, due to lack of data or conditions not met for melt detection. Graph **e)** shows the same time series of 12-hour snow depth measurements with all five melt indicators plotted above for comparisons.

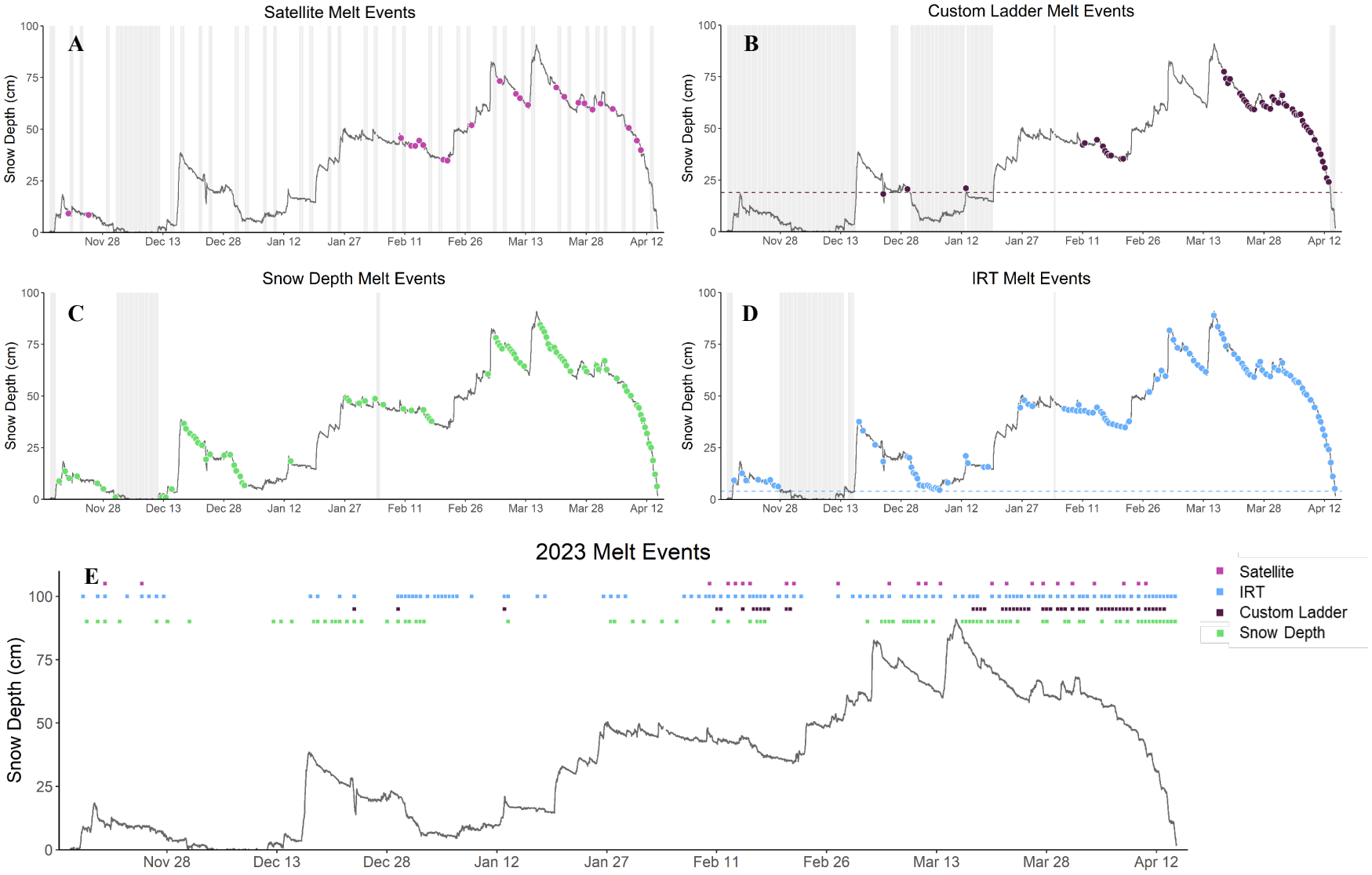
Satellite Melt Events
A
Custom Ladder Melt Events
B
Snow Depth Melt Events
C
IRT Melt Events
D
2023 Melt Events
E
Snow Depth (cm)
0
25
50
75
100
Nov 28
Dec 13
Dec 28
Jan 12
Jan 27
Feb 11
Feb 26
Mar 13
Mar 28
Apr 12
Satellite
IRT
Custom Ladder
Snow Depth

Figure 9: Timeseries of 10-minute snow depth measurements at SRRW for the 2022-2023 winter with **a)** satellite, **b)** custom ladder, **c)** snow depth, and **d)** IRT melt events. Horizontal dashed lines in **b)** indicate 20 cm snow depth thresholds necessary for the custom temperature ladder melt detection. Grey shaded time periods on **a)** – **d)** indicate times when each respective melt indicator is NA, due to lack of data or conditions not met for melt detection. Graph **e)** shows the same time series of 10-minute snow depth measurements with all four melt indicators plotted above for comparison.

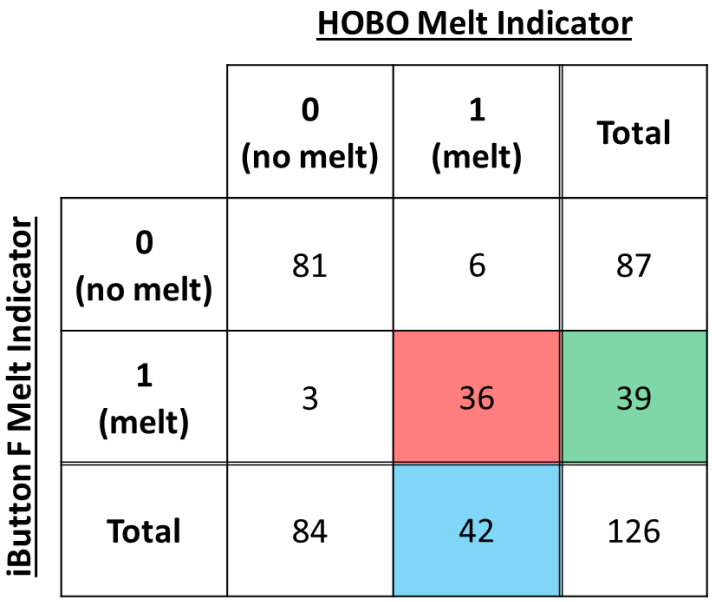

Figure 10: Example confusion matrix for comparing SRRW HOBO temperature ladder melt events with the iButton F temperature ladder melt events. Red shows total number of matching melt events (TP), green shows total number iButton F melt events, and blue shows total number of HOBO melt events.

Table 2: SRRW sensitivities (TPR) between in-situ melt indicators. Each row and column indicate a different combination of data. Agreements are calculated using the total number of the column name for total melt events. **(a)** WY 2022, **(b)** WY 2023.

Assumed to be "True"

2022	**SD**	**iButton S**	**iButton F**	**HOBO**
SD	-	59.0%	63.1%	57.1%
iButton S	52.5%	-	95.0%	90.4%
iButton F	54.5%	97.4%	-	85.7%
HOBO	54.5%	95.0%	92.3%	-

Assumed to be "True"

2023	**SD**	**IRT**	**Custom Ladder**
SD	-	48.2%	53.8%
IRT	66.3%	-	76.9%
Custom Ladder	42.4%	48.8%	-

Table 3: Summary of Sleeper's River Research Watershed snowmelt detection results for 2022 and 2023, including total melt events and agreements between satellite and in-situ melt indicators. Exact Binomial Tests were performed to determine if any agreements could be due to random chance. Sensitivities in black indicate they are higher than what would be expected from random chance, while grey indicates they are not.

	# of Melts Detected			**Sensitivity ("True" Melts)**	
In-Situ Melt Indicator	***In-Situ***	***Satellite***	***Both***	***TPR Satellite***	***TPR In-Situ***
2022					
Snow Depth	51	13	10	77%	20%
iButton S Ladder	31	11	8	73%	26%
iButton F Ladder	31	11	9	82%	29%
HOBO Ladder	34	11	8	73%	24%
2023					
Snow Depth	63	24	11	46%	17%
IRT	86	24	23	96%	27%
Custom Ladder	38	22	9	41%	24%

Table 4: Average sensitivity (rate of true positive) for SNOTEL analysis for the SD (snow depth), SWE, and combined datasets. The number of sites in each dataset is also listed. Sensitivity was calculated first assuming satellite data is "true" and then assuming in-situ is "true".

		Average Sensitivities	
In-Situ Melt Indicator	**# of Sites**	**Satellite**	**In-Situ**
SD (all)	481	53.4%	43.0%
SD (combined)	444	53.4%	43.2%
SWE (all)	563	27.8%	39.7%
SWE (combined)	444	27.6%	39.2%

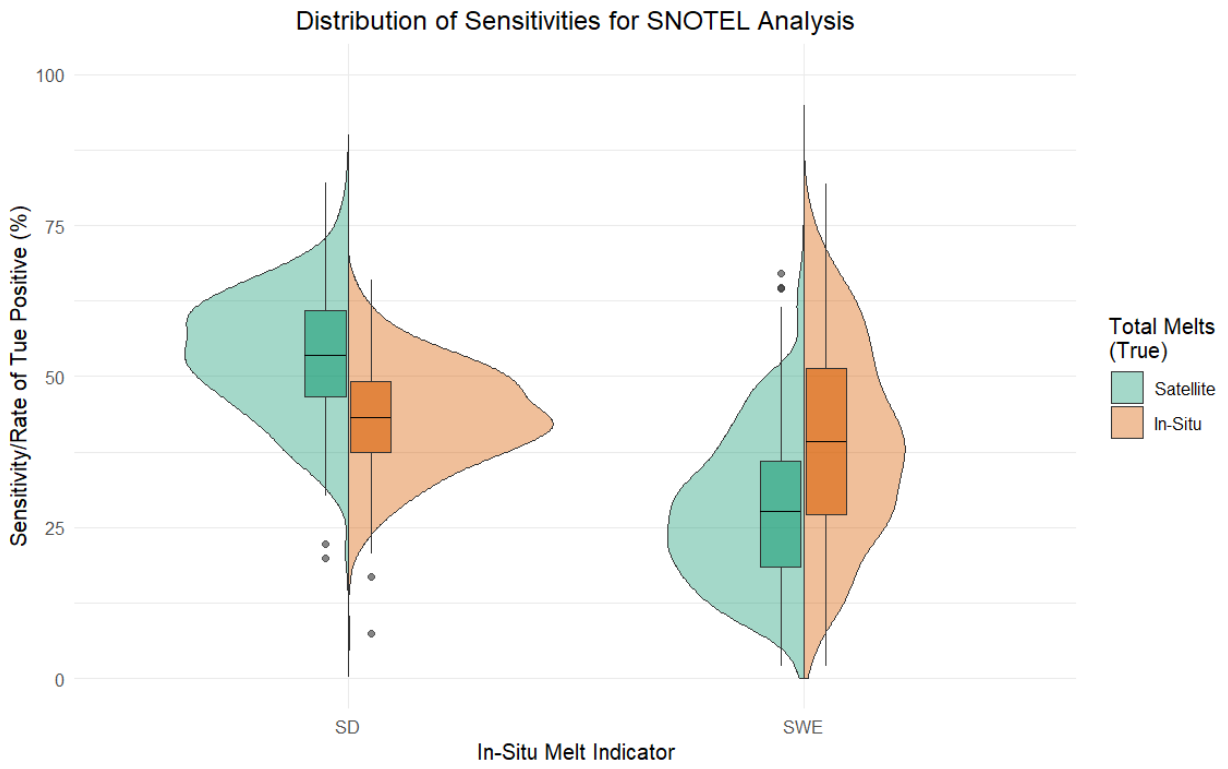

Figure 11: Distributions of the daily sensitivity (TPR) statistic for all snow stations (444). "SD" refers to the comparison of snow depth and satellite melt events and "SWE" refers to the comparison of SWE and satellite melt events. The percent of true positive melts was calculated for the total number of satellite melt events (blue/green) and for the total number of in-situ melt events (orange). Horizontal line within boxplots indicates the mean of the dataset rather than the median.

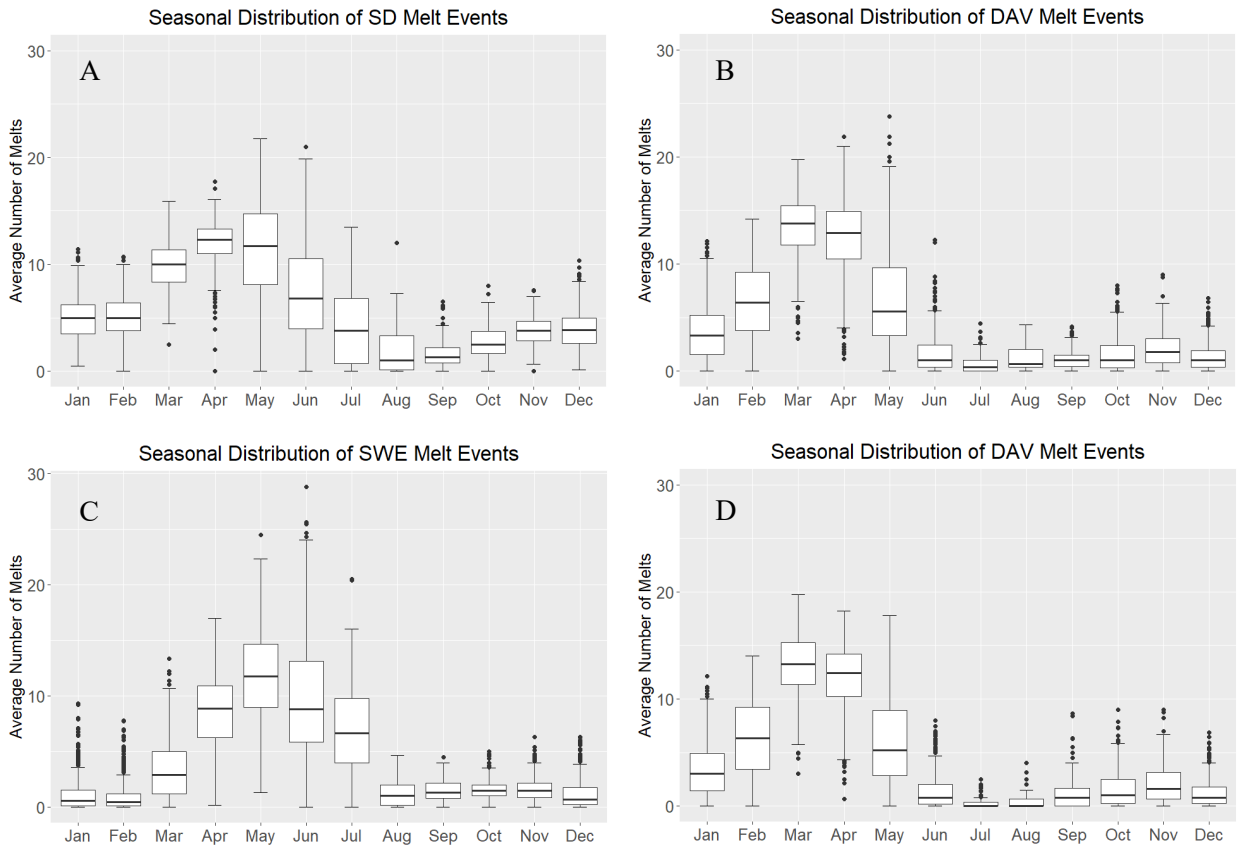

Figure 12: Seasonal distribution of melt detection frequency for: **(a)** Snow Depth melts, **(b)** satellite melts (DAV) from the SD dataset, **(c)** SWE melts, and **(d)** satellite melts from the SWE dataset. Each datapoint is the average number of melt events that occur in that month for a specific site.

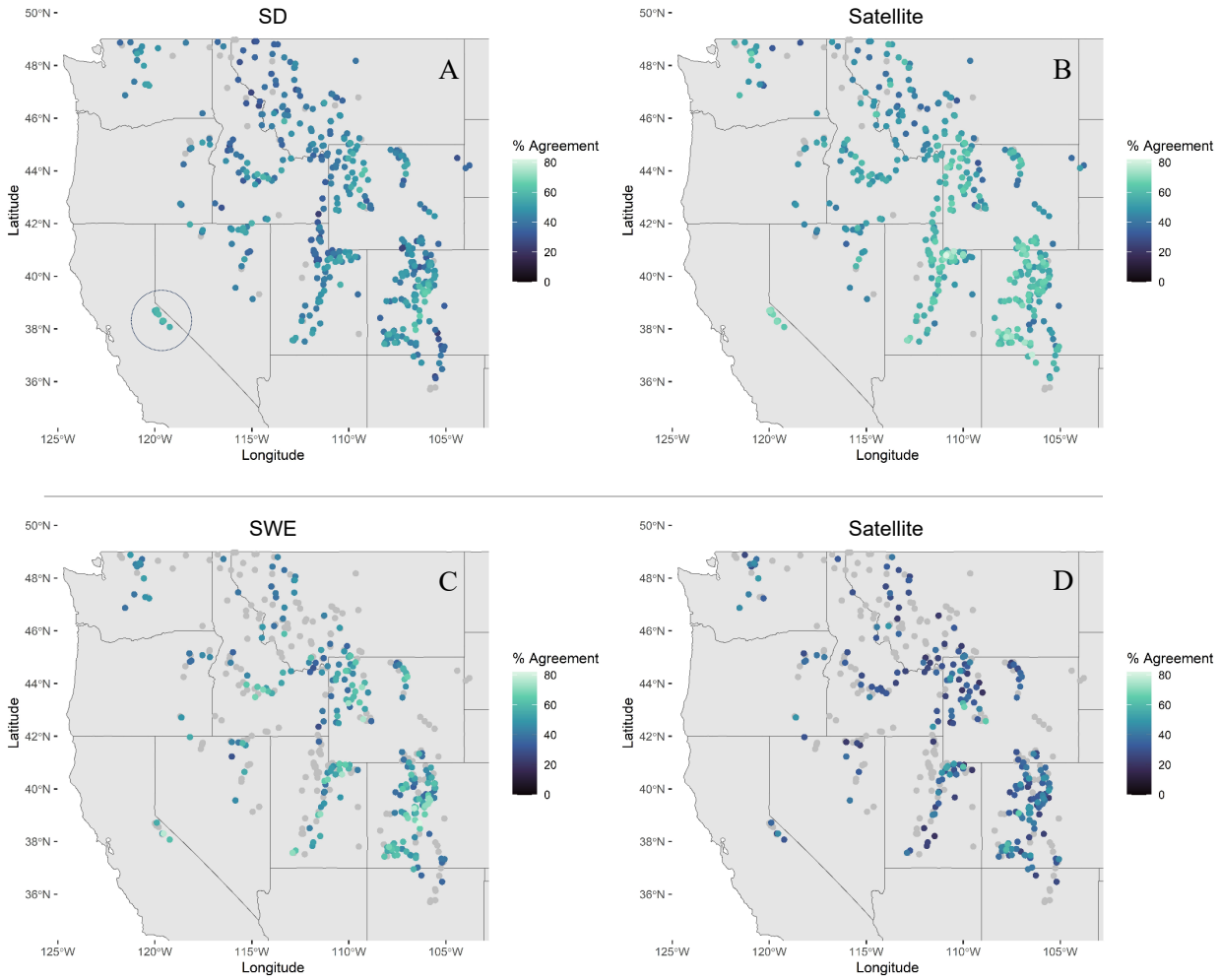

Figure 13: Map of SNOTEL sites and their sensitivities for the snow depth analysis (left) and SWE analysis (right), assuming that the in-situ melt indicator is "true" (top), and assuming the satellite melt indicator is "true" (bottom). **a)** Group of sites located in the Sierra Nevada Mountains are circled to show regional pattern of higher agreement between snow depth and satellite melt indicators.

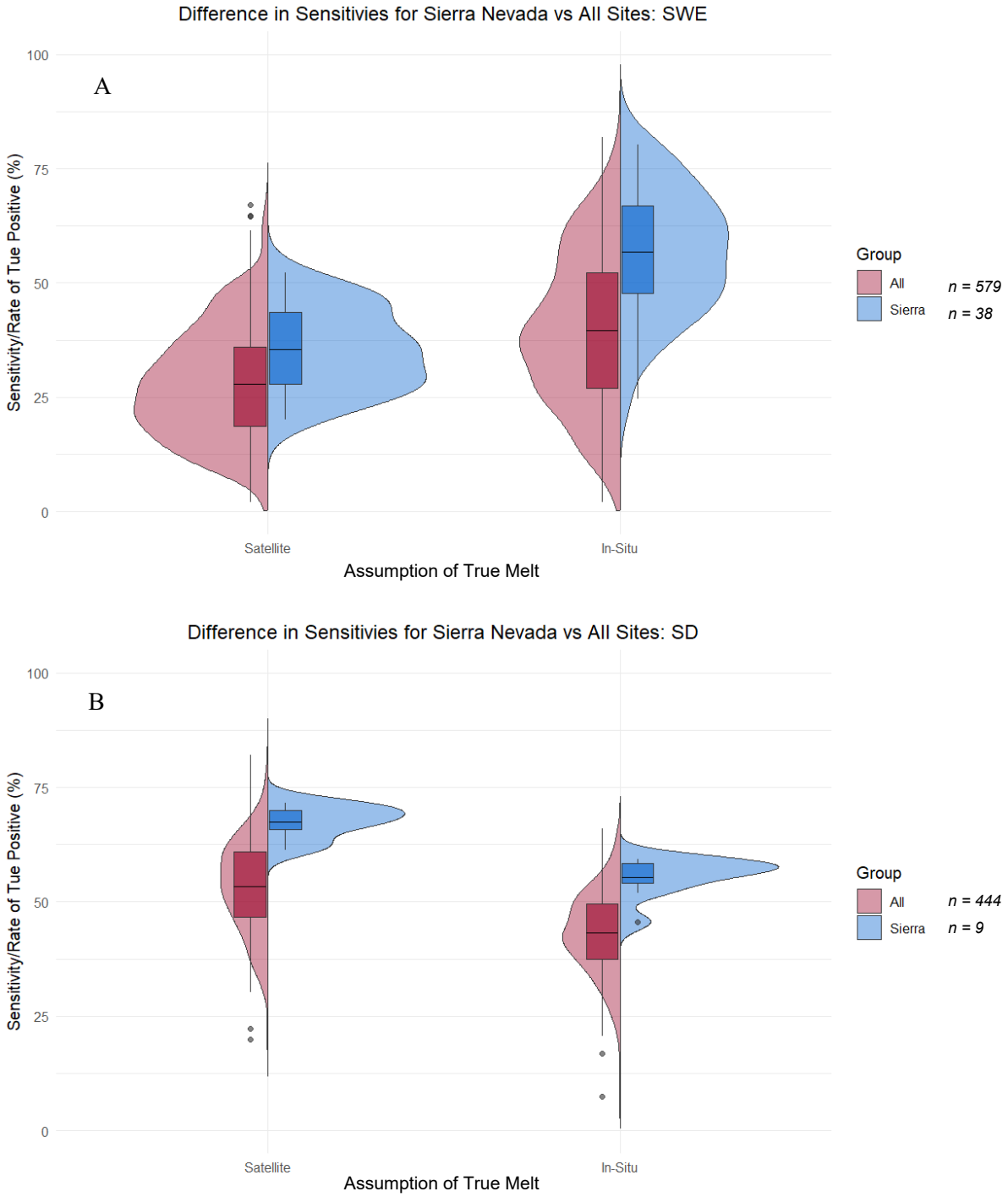

Figure 14: a) Distributions of satellite and SWE sensitivities for all sites (red) compared to snow stations located within the Sierra Nevada Mountain Range (blue). **b)** Distributions of satellite and snow depth sensitivities for all sites (red) compared to snow stations located within the Sierra Nevada Mountain Range (blue). Kruskal-Wallis tests indicate that the Sierra Nevada snow stations have significantly higher agreements for all agreement statistics ($p > 0.05$).

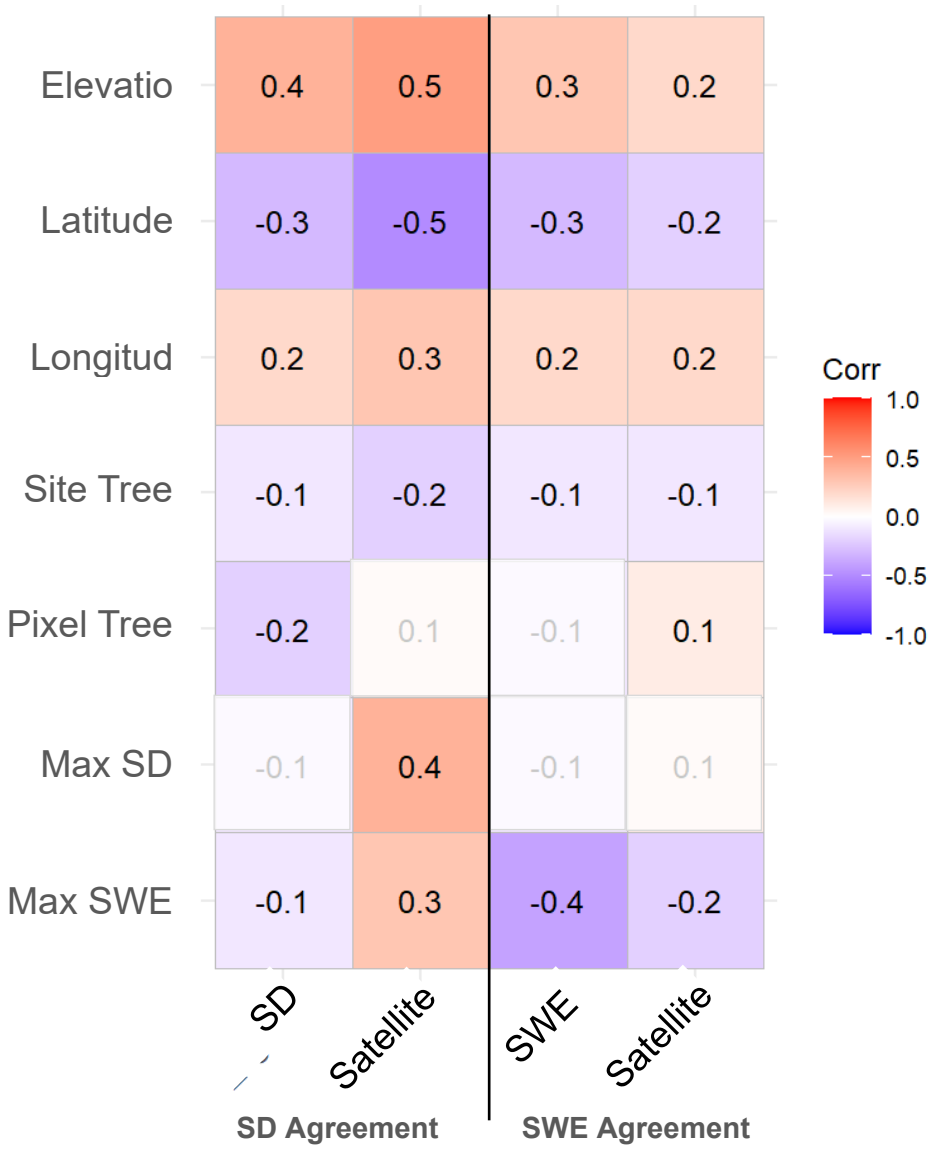

Figure 15: Calculated spearman correlations between agreement statistics and site characteristics using the combined agreement dataset (n = 444). Elevation, latitude, longitude, and site tree cover refer to characteristics of the snow station site itself. Pixel tree cover refers to the tree cover percent of the entire AMSR-E pixel containing the snow station. The variable "Max SD" is the average yearly snow depth maximum recorded for each site, and same for the SWE. Color scale indicates direction and magnitude of correlation. Grey numbers indicate correlation was not found to be significant, with $p < 0.05$. The first two columns are for agreements between snow depth and satellite melt indicators, the second two columns are for SWE and satellite agreements. SD/SWE refer to rate of true positive (TPR) assuming ground-detected melt events are true, and "Satellite" refers to the TPR calculated assuming that the satellite-detected melt events are true.

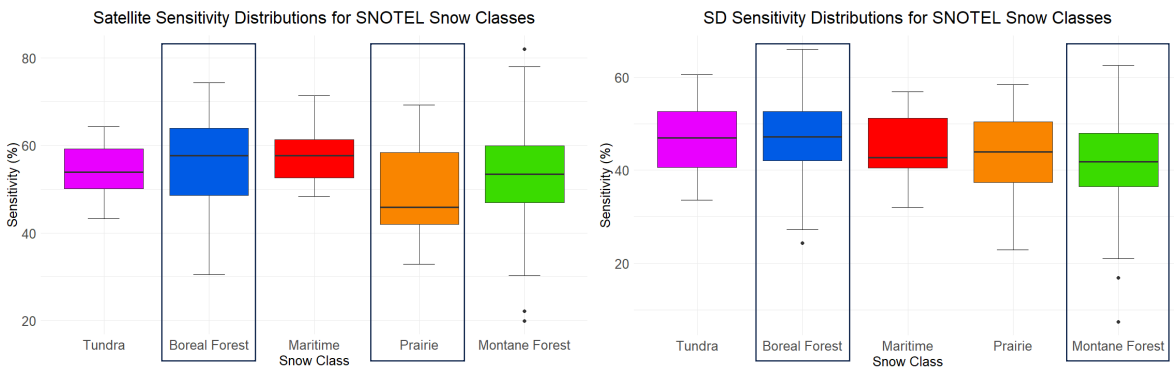

Figure 16: Agreements by snow class. **(a)** Distributions of agreement between snow depth and satellite snowmelt indicators calculated assuming the satellite is detecting true melt events ($TPR_{Satellite}$). **(b)** Agreement between snow depth and satellite indicators calculated assuming satellite-detected melt events are true (TPR_{SD}). Kruskal-Wallis tests indicate that SD agreements show statistically significant differences between snow class groups, while SWE agreements showed no significant differences and are therefore not pictured. A Dunn's Test indicates that for the $TPR_{Satellite}$ **(a)**, Boreal Forest and Montane Forest have significantly different means, and for the TPR_{SD} **(b)**, only Boreal Forest and Prairie have significantly different means ($p > 0.05$). The snow class group "Ephemeral" was excluded due to lack of data.

References

Abdalati, W., & Steffen, K. (1995). Passive microwave-derived snow melt regions on the Greenland Ice Sheet. *Geophysical Research Letters*, *22*(7), 787–790. https://doi.org/10.1029/95GL00433

Adam, J. C., Hamlet, A. F., & Lettenmaier, D. P. (2009). Implications of global climate change for snowmelt hydrology in the twenty-first century. *Hydrological Processes*, *23*(7), 962–972. https://doi.org/10.1002/hyp.7201

Apgar, J. D., Ramage, J. M., McKenney, R. A., & Maltais, P. (2007). AMSR-E algorithm for snowmelt onset detection in sub-arctic heterogeneous terrain. *Hydrological Processes*, *21*(12), 1587–1596. https://doi.org/10.1002/hyp.6721

Apogee. (2015). *Apogee Broadband Infrared Radiometer Model SI-111 Manual*. https://www.apogeeinstruments.com/content/SI-100-manual.pdf/

Barnett, T. P., Adam, J. C., & Lettenmaier, D. P. (2005). Potential impacts of a warming climate on water availability in snow-dominated regions. *Nature*, *438*(7066), Article 7066. https://doi.org/10.1038/nature04141

Blöschl, G. (1999). Scaling issues in snow hydrology. *Hydrological Processes*, *13*(14–15), 2149–2175. https://doi.org/10.1002/(SICI)1099-1085(199910)13:14/15<2149::AID-HYP847>3.0.CO;2-8

Chang, A. T. C., Foster, J. L., & Hall, D. K. (1987). Nimbus-7 SMMR Derived Global Snow Cover Parameters. *Annals of Glaciology*, *9*, 39–44. https://doi.org/10.3189/S0260305500200736

Chang, A. T. C., Foster, J. L., & Hall, D. K. (1996). Effects of Forest on the Snow Parameters Derived from Microwave Measurements during the Boreas Winter Field Campaign. *Hydrological Processes*, *10*, 1565–1574. https://doi.org/10.1002/(SICI)1099-1085(199612)10:12<1565::AID-HYP501>3.0.CO;2-5

Chang, A. T. C., Gloersen, P., Schmugge, T., Wilheit, T. T., & Zwally, H. J. (1976). Microwave emission from snow and glacier ice. *Journal of Glaciology*, *16*, 23–39. https://doi.org/10.1017/S0022143000031415

Cline, D. W. (1997). Snow surface energy exchanges and snowmelt at a continental, midlatitude Alpine site. *Water Resources Research*, *33*, 689–701. https://doi.org/10.1029/97WR00026

Clow, D. W. (2010). Changes in the Timing of Snowmelt and Streamflow in Colorado: A Response to Recent Warming. *Journal of Climate*, *23*(9), 2293–2306. https://doi.org/10.1175/2009JCLI2951.1

Conde, V., Nico, G., Mateus, P., Catalão, J., Kontu, A., & Gritsevich, M. (2019). On The Estimation of Temporal Changes of Snow Water Equivalent by Spaceborne Sar Interferometry: A New Application for the Sentinel-1 Mission. *Journal of Hydrology and Hydromechanics*, *67*(1), 93–100. https://doi.org/10.2478/johh-2018-0003

Dingman, S. L. (2014). *Physical Hydrology, Third Edition* (3rd edition). Waveland Press, Inc.

Dolant, C., Langlois, A., Montpetit, B., Brucker, L., Roy, A., & Royer, A. (2016). Development of a rain-on-snow detection algorithm using passive microwave radiometry. *Hydrological Processes*, *30*. https://doi.org/10.1002/hyp.10828

Dong, J., Walker, J. P., & Houser, P. R. (2005). Factors affecting remotely sensed snow water equivalent uncertainty. *Remote Sensing of Environment*, *97*(1), 68–82. https://doi.org/10.1016/j.rse.2005.04.010

Dozier, J. (2011). Mountain hydrology, snow color, and the fourth paradigm. *Eos, Transactions American Geophysical Union*, *92*(43), 373–374. https://doi.org/10.1029/2011EO430001

Fierz, C., Armstrong, R. L., Durand, Y., Etchevers, P., Greene, E., McClung, D. M., Nishimura, K., Satyawali, P. K., & Sokratov, S. A. (2009). *The international classification for seasonal snow on the ground. Prepared by the ICSI-UCCS-IACS working group on snow classification*. https://www.dora.lib4ri.ch/wsl/islandora/object/wsl%3A10162/

Fleming, S. W., Zukiewicz, L., Strobel, M. L., Hofman, H., & Goodbody, A. G. (2023). SNO^{TEL}, the Soil Climate Analysis Network, and water supply forecasting at the Natural Resources Conservation Service: Past, present, and future. *JAWRA Journal of the American Water Resources Association*, *59*(4), 585–599. https://doi.org/10.1111/1752-1688.13104

Foster, J. L., Chang, A. T. C., Hall, D. K., & Rango, A. (1991). Derivation of Snow Water Equivalent in Boreal Forests Using Microwave Radiometry. *Arctic*, *44*, 147–152.

Foster, J. L., Hall, D. K., Eylander, J. B., Riggs, G. A., Nghiem, S. V., Tedesco, M., Kim, E., Montesano, P. M., Kelly, R. E. J., Casey, K. A., & Choudhury, B. (2011). A blended global snow product using visible, passive microwave and scatterometer satellite data. *International Journal of Remote Sensing*, *32*(5), 1371–1395. https://doi.org/10.1080/01431160903548013

Foster, J. L., Sun, C., Walker, J. P., Kelly, R., Chang, A., Dong, J., & Powell, H. (2005). Quantifying the uncertainty in passive microwave snow water equivalent observations. *Remote Sensing of Environment*, *94*(2), 187–203. https://doi.org/10.1016/j.rse.2004.09.012

Frei, A., Tedesco, M., Lee, S., Foster, J., Hall, D. K., Kelly, R., & Robinson, D. A. (2012). A review of global satellite-derived snow products. *Advances in Space Research*, *50*(8), 1007–1029. https://doi.org/10.1016/j.asr.2011.12.021

Freudiger, D., Kohn, I., Stahl, K., & Weiler, M. (2014). Large-scale analysis of changing frequencies of rain-on-snow events with flood-generation potential. *Hydrology and Earth System Sciences*, *18*(7), 2695–2709. https://doi.org/10.5194/hess-18-2695-2014

Grenfell, T. C., & Putkonen, J. (2008). A method for the detection of the severe rain-on-snow event on Banks Island, October 2003, using passive microwave remote sensing. *Water Resources Research*, *44*(3). https://doi.org/10.1029/2007WR005929

Hallikainen, M., Lemmetyinen, J., & Jiang, L. (2018). 4.09—Snow Properties From Passive Microwave. In S. Liang (Ed.), *Comprehensive Remote Sensing* (pp. 224–236). Elsevier. https://doi.org/10.1016/B978-0-12-409548-9.10358-6

Heldmyer, A., Livneh, B., Molotch, N., & Rajagopalan, B. (2021). Investigating the Relationship Between Peak Snow-Water Equivalent and Snow Timing Indices in the Western United States and Alaska. *Water Resources Research*, *57*(5), e2020WR029395. https://doi.org/10.1029/2020WR029395

Helgason, W., & Pomeroy, J. (2012). Problems Closing the Energy Balance over a Homogeneous Snow Cover during Midwinter. *Journal of Hydrometeorology*, *13*(2), 557–572. https://doi.org/10.1175/JHM-D-11-0135.1

Hiemstra, C. A., Liston, G. E., & Reiners, W. A. (2006). Observing, modelling, and validating snow redistribution by wind in a Wyoming upper treeline landscape. *Ecological Modelling*, *197*(1), 35–51. https://doi.org/10.1016/j.ecolmodel.2006.03.005

Hori, M., Aoki, T., Tanikawa, T., Hachikubo, A., Sugiura, K., Kuchiki, K., & Niwano, M. (2013). Modeling angular-dependent spectral emissivity of snow and ice in the thermal

infrared atmospheric window. *Applied Optics*, *52*(30), 7243–7255. https://doi.org/10.1364/AO.52.007243

Ingólfsson, Ö., Engineering, P., Grímsdóttir, H., & Jónsson, M. H. (2012). *MONITORING SNOWPACK TEMPERATURE GRADIENT USING AUTOMATIC SNOW DEPTH SENSOR*.

Johnson, M. T., Ramage, J., Troy, T. J., & Brodzik, M. J. (2020). Snowmelt Detection with Calibrated, Enhanced-Resolution Brightness Temperatures (CETB) in Colorado Watersheds. *Water Resources Research*, *56*(1), e2018WR024542. https://doi.org/10.1029/2018WR024542

Kinar, N. J., & Pomeroy, J. W. (2015). Measurement of the physical properties of the snowpack. *Reviews of Geophysics*, *53*(2), 481–544. https://doi.org/10.1002/2015RG000481

Kopp, M., Tuo, Y., & Disse, M. (2019). Fully automated snow depth measurements from time-lapse images applying a convolutional neural network. *Science of The Total Environment*, *697*, 134213. https://doi.org/10.1016/j.scitotenv.2019.134213

Langlois, A., Royer, A., Derksen, C., Montpetit, B., Dupont, F., & Goïta, K. (2012). Coupling the snow thermodynamic model SNOWPACK with the microwave emission model of layered snowpacks for subarctic and arctic snow water equivalent retrievals. *Water Resources Research*, *48*(12). https://doi.org/10.1029/2012WR012133

Li, D., Durand, M., & Margulis, S. A. (2012). Potential for hydrologic characterization of deep mountain snowpack via passive microwave remote sensing in the Kern River basin, Sierra Nevada, USA. *Remote Sensing of Environment*, *125*, 34–48. https://doi.org/10.1016/j.rse.2012.06.027

Li, D., Wrzesien, M. L., Durand, M., Adam, J., & Lettenmaier, D. P. (2017). How much runoff originates as snow in the western United States, and how will that change in the future? *Geophysical Research Letters*, *44*(12), 6163–6172. https://doi.org/10.1002/2017GL073551

Lund, J., Forster, R. R., Deeb, E. J., Liston, G. E., Skiles, S. M., & Marshall, H.-P. (2022). Interpreting Sentinel-1 SAR Backscatter Signals of Snowpack Surface Melt/Freeze, Warming, and Ripening, through Field Measurements and Physically-Based SnowModel. *Remote Sensing*, *14*(16), Article 16. https://doi.org/10.3390/rs14164002

Marks, D., & Dozier, J. (1992). Climate and energy exchange at the snow surface in the Alpine Region of the Sierra Nevada: 2. Snow cover energy balance. *Water Resources Research*, *28*(11), 3043–3054. https://doi.org/10.1029/92WR01483

Mätzler, C. (1987). Applications of the interaction of microwaves with the natural snow cover. *Remote Sensing Reviews*, *2*(2), 259–387. https://doi.org/10.1080/02757258709532086

Mätzler, C. (1994). Passive Microwave Signatures of Landscapes in Winter. *Meteorology and Atmospheric Physics*, *54*(1–4), Article 1–4.

McGurk, B. (1983). *Snow temperature profiles in the Central Sierra Nevada*. 9–81.

Mellor, M. (1964). Snow and ice on the earth's surface. In *This Digital Resource was created from scans of the Print Resource* [Report]. Cold Regions Research and Engineering Laboratory (U.S.). https://erdc-library.erdc.dren.mil/jspui/handle/11681/2630

Meromy, L., Molotch, N. P., Link, T. E., Fassnacht, S. R., & Rice, R. (2013). Subgrid variability of snow water equivalent at operational snow stations in the western USA. *Hydrological Processes*, *27*(17), 2383–2400. https://doi.org/10.1002/hyp.9355

Mitchell, K. E., Lohmann, D., Houser, P. R., Wood, E. F., Schaake, J. C., Robock, A., Cosgrove, B. A., Sheffield, J., Duan, Q., Luo, L., Higgins, R. W., Pinker, R. T., Tarpley, J. D.,

Lettenmaier, D. P., Marshall, C. H., Entin, J. K., Pan, M., Shi, W., Koren, V., … Bailey, A. A. (2004). The multi-institution North American Land Data Assimilation System (NLDAS): Utilizing multiple GCIP products and partners in a continental distributed hydrological modeling system. *Journal of Geophysical Research: Atmospheres*, *109*(D7). https://doi.org/10.1029/2003JD003823

Musselman, K. N., Addor, N., Vano, J. A., & Molotch, N. P. (2021). Winter melt trends portend widespread declines in snow water resources. *Nature Climate Change*, *11*(5), Article 5. https://doi.org/10.1038/s41558-021-01014-9

Musselman, K. N., Clark, M. P., Liu, C., Ikeda, K., & Rasmussen, R. (2017). Slower snowmelt in a warmer world. *Nature Climate Change*, *7*(3), Article 3. https://doi.org/10.1038/nclimate3225

Musselman, K. N., Lehner, F., Ikeda, K., Clark, M. P., Prein, A. F., Liu, C., Barlage, M., & Rasmussen, R. (2018). Projected increases and shifts in rain-on-snow flood risk over western North America. *Nature Climate Change*, *8*(9), Article 9. https://doi.org/10.1038/s41558-018-0236-4

Pérez-Díaz, C. L., Lakhankar, T., Romanov, P., Muñoz, J., Khanbilvardi, R., & Yu, Y. (2017). Evaluation of MODIS land surface temperature with in-situ snow surface temperature from CREST-SAFE. *International Journal of Remote Sensing*, *38*(16), 4722–4740. https://doi.org/10.1080/01431161.2017.1331055

Pomeroy, J. W., Gray, D. M., Shook, K. R., Toth, B., Essery, R. L. H., Pietroniro, A., & Hedstrom, N. (1998). An evaluation of snow accumulation and ablation processes for land surface modelling. *Hydrological Processes*, *12*(15), 2339–2367. https://doi.org/10.1002/(SICI)1099-1085(199812)12:15<2339::AID-HYP800>3.0.CO;2-L

Porter, V. M., Shanley, J. B., Sebestyen, S. D., & Liu, F. (2022). Controls on decadal, annual, and seasonal concentration-discharge relationships in the SLEEPERS RIVER RESEARCH WATERSHED , VERMONT, NORTHEASTERN UNITED STATES. *Hydrological Processes*, *36*(3), e14559. https://doi.org/10.1002/hyp.14559

Putkonen, J., Grenfell, T. C., Rennert, K., Bitz, C., Jacobson, P., & Russell, D. (2009). Rain on Snow: Little Understood Killer in the North. *Eos, Transactions American Geophysical Union*, *90*(26), 221–222. https://doi.org/10.1029/2009EO260002

R. W. Gerdel. (1944). Snow-temperature studies and apparatus at the Soda Springs, California, cooperative snow-research project. *Eos, Transactions American Geophysical Union*, *25*(1), 118–122. https://doi.org/10.1029/TR025i001p00118

Ramage, J. M., & Isacks, B. L. (2002). Determination of melt-onset and refreeze timing on southeast Alaskan icefields using SSM/I diurnal amplitude variations. *Annals of Glaciology*, *34*, 391–398. https://doi.org/10.3189/172756402781817761

Ramage, J., & Semmens, K. A. (2012). Reconstructing snowmelt runoff in the Yukon River basin using the SWEHydro model and AMSR-E observations. *Hydrological Processes*, *26*(17), 2563–2572. https://doi.org/10.1002/hyp.9226

Schaefer, G. L. (2000). *SNOTEL (SNOwpack TELemetry)*.

Schweizer, J., Mitterer, C., Reuter, B., & Techel, F. (2021). Avalanche danger level characteristics from field observations of snow instability. *The Cryosphere*, *15*(7), 3293–3315. https://doi.org/10.5194/tc-15-3293-2021

Serreze, M. C., Clark, M. P., Armstrong, R. L., McGinnis, D. A., & Pulwarty, R. S. (1999). Characteristics of the western United States snowpack from snowpack telemetry

(SNO^{TEL}) data. *Water Resources Research*, *35*(7), 2145–2160. https://doi.org/10.1029/1999WR900090

Sexstone, G. A., Fassnacht, S. R., López-Moreno, J. I., & Hiemstra, C. A. (2016). *Subgrid snow depth coefficient of variation within complex mountainous terrain* [Preprint]. Seasonal Snow. https://doi.org/10.5194/tc-2016-188

Shanley, J. B., & Chalmers, A. (1999). The effect of frozen soil on snowmelt runoff at Sleepers River, Vermont. *Hydrological Processes*, *13*(12–13), 1843–1857. https://doi.org/10.1002/(SICI)1099-1085(199909)13:12/13<1843::AID-HYP879>3.0.CO;2-G

Stewart, I. T. (2009). Changes in snowpack and snowmelt runoff for key mountain regions. *Hydrological Processes*, *23*(1), 78–94. https://doi.org/10.1002/hyp.7128

Stiles, W. H., & Ulaby, F. T. (1980). The active and passive microwave response to snow parameters: 1. Wetness. *Journal of Geophysical Research: Oceans*, *85*(C2), 1037–1044. https://doi.org/10.1029/JC085iC02p01037

Sturm, M., Holmgren, J., & Liston, G. E. (1995). A Seasonal Snow Cover Classification System for Local to Global Applications. *Journal of Climate*, *8*(5), 1261–1283. https://doi.org/10.1175/1520-0442(1995)008<1261:ASSCCS>2.0.CO;2

Sturm, M., & Johnson, J. B. (1991). Natural convection in the subarctic snow cover. *Journal of Geophysical Research: Solid Earth*, *96*(B7), 11657–11671. https://doi.org/10.1029/91JB00895

Sturm, M., & Liston, G. E. (2021). Revisiting the Global Seasonal Snow Classification: An Updated Dataset for Earth System Applications. *Journal of Hydrometeorology*, *22*(11), 2917–2938. https://doi.org/10.1175/JHM-D-21-0070.1

Sun, W.-Y., & Chern, J.-D. (2005). Validation of A One-Dimensional Snow-Land Surface Model at the Sleepers River Watershed. *Boundary-Layer Meteorology*, *116*(1), 95–115. https://doi.org/10.1007/s10546-004-7741-x

Tanniru, S., & Ramsankaran, R. (2023). Passive Microwave Remote Sensing of Snow Depth: Techniques, Challenges and Future Directions. *Remote Sensing*, *15*(4), Article 4. https://doi.org/10.3390/rs15041052

Tedesco, M. (2007). Snowmelt detection over the Greenland ice sheet from SSM/I brightness temperature daily variations. *Geophysical Research Letters*, *34*(2). https://doi.org/10.1029/2006GL028466

Tedesco, M., Brodzik, M., Armstrong, R., Savoie, M., & Ramage, J. (2009). Pan arctic terrestrial snowmelt trends (1979–2008) from spaceborne passive microwave data and correlation with the Arctic Oscillation. *Geophysical Research Letters*, *36*(21). https://doi.org/10.1029/2009GL039672

Tuttle, S. E., & Jacobs, J. M. (2019). Enhanced Identification of Snow Melt and Refreeze Events From Passive Microwave Brightness Temperature Using Air Temperature. *Water Resources Research*, *55*(4), 3248–3265. https://doi.org/10.1029/2018WR023995

Vuyovich, C. M., Jacobs, J. M., Hiemstra, C. A., & Deeb, E. J. (2017). Effect of spatial variability of wet snow on modeled and observed microwave emissions. *Remote Sensing of Environment*, *198*, 310–320. https://doi.org/10.1016/j.rse.2017.06.016

Walker, A. E., & Goodison, B. E. (1993). Discrimination of a wet snow cover using passive microwave satellite data. *Annals of Glaciology*, *17*, 307–311. https://doi.org/10.3189/S026030550001301X

Watson, F. G. R., Anderson, T. N., Newman, W. B., Alexander, S. E., & Garrott, R. A. (2006). Optimal sampling schemes for estimating mean snow water equivalents in stratified heterogeneous landscapes. *Journal of Hydrology*, *328*(3), 432–452. https://doi.org/10.1016/j.jhydrol.2005.12.032

Zheng, L., Zhou, C., Liu, R., & Sun, Q. (2018). Antarctic Snowmelt Detected by Diurnal Variations of AMSR-E Brightness Temperature. *Remote Sensing*, *10*(9), Article 9. https://doi.org/10.3390/rs10091391

Glossary

AMSR2 – Advanced Microwave Scanning Radiometer 2

AMSR-E – Advanced Microwave Scanning Radiometer for EOS

DAV – Diurnal amplitude variation

IRT – Infrared Radiometer

LWC – Liquid water content

NLDAS-2 – North American Land Data Assimilation System, Phase 2

PMW – Passive Microwave

SD – Snow depth

SNOTEL – SNOwpack TELemetry

SPA-2 – Snow Pack Analyzer-2

SRRW – Sleeper's River Research Watershed, VT

SSM/I – Special Sensor Microwave Imager

SSMIS – Special Sensor Microwave Imager/Sounder

SWE – Snow water equivalent

Curriculum Vita

EDUCATION

M.S. in Earth Science; GPA: 4.0 ***December 2023***
Syracuse University, Department of Earth and Environmental Sciences (EES)

B.S. in Geology / B.S. in GIS; GPA: 3.90 ***May 2020***
Hofstra University
- Graduated Summa Cum Laude, HU Honors College Associate
- Minored in Mathematics and Meteorology

RESEARCH EXPERIENCE

Master's Thesis (supervisor Dr. Sam Tuttle) ***Fall 2021 - present***
Department of EES, Syracuse University
Thesis: Evaluating Passive Microwave Snowmelt Detection Methods with Ground Snow Data
- Compared snowmelt events detected by the AMSR-E satellite to in-situ data from snow field stations (SNOTEL)
- Used R programming to evaluate accuracy and viability of satellite detection methods as a function of different snowpack characteristics
- Presented findings at local and national conferences, and intend to prepare a manuscript for peer-reviewed journal submission

Graduate Research Project (supervisor Dr. Elizabeth Carter) ***Fall 2021***
Department of EES, Syracuse University
Project: Application of InSAR to Measure Ice Jam Development based on Vertical Displacement on the Mohawk River, NY
- Compared vertical displacement from InSAR data against changes in stage height at USGS stream gauges before, during, and after a historic ice jam flood event
- Used Python and ArcGIS to perform linear regression to determine if there was a statistically significant relationship
- Interpreted results in relation to upstream/downstream flow and prepared final research paper

Research Project (supervisor Dr. Antonios Marsellos) ***Spring 2019***
Department of Geology, Hofstra University
Project: Multivariable Statistical Analysis of Groundwater Elevation Fluctuations
- Collected and manipulated data in SPSS, KNIME, and Excel
- Performed time series and regression models to predict groundwater elevation from various environmental variables
- Used Global Mapper and Google Earth Pro to create DSMs and DTMs

Research Project (supervisor Dr. Antonios Marsellos) ***Spring 2018***
Department of Geology, Hofstra University
Project: An Approach to Determine Flood Vulnerable Sites using LiDAR and Flood Simulations
- Simulated historic flood in Oneida County, NY, using Global Mapper and LiDAR DEM

- Collected images of flood and found GPS locations of each using Google Earth Pro
- Compared accuracy of flood simulation using DTM versus DSM

Research Assistant (supervisor Dr. Jase Bernhardt ***2017 – 2019***
Department of Geology, Hofstra University
Project: Communicating Hurricane Risk with Virtual Reality

- Developed and distributed surveys to students and local communities to test the VR simulation and its effectiveness
- Analyzed quantitative and qualitative survey data using excel
- Prepared final reports and presented findings at national conferences

Research Assistant (supervisor Dr. Jase Bernhardt) ***2019***
Department of Geology, Hofstra University
Project: Using Virtual Reality as an Educational Tool for Rip Currents

- Developed/distributed surveys to test the knowledge and response to a rip current simulation
- Transcribed recorded survey questions into an excel format to be analyzed

FIELD EXPERIENCE

Graduate Field Assistant (supervisor Dr. Sam Tuttle) ***Winter 2021 - present***
Department of EES, Syracuse University
Field Site: USGS Sleepers River Research Watershed, VT

- Assisted with snow field station setup for two winters at Sleeper's River Research Watershed, VT
- Calibrated and programmed 40+ iButton temperature sensors to collect temperature within vertical snow profile
- Assisted with programming, building, and installing temperature ladders for comparative snowpack temperature profiles, including using Campbell Scientific datalogger/multiplexer and HOBO loggers
- Installed Snowpack Analyzer-2 to record parameters such as snow water equivalent, liquid water content, and snow depth
- Plan to assist with field snow sampling in the Adirondacks this winter

Field Research Assistant (supervisor Dr. Antonios Marsellos ***July 2019***
Department of Geology, Hofstra University, Greece
Field Sites: Athens, Milos, Santorini, & Nisyros, Greece

- Assembled and replaced equipment at monitoring stations
- Collected and recorded soil samples and GPS coordinates from each site
- Assisted in collecting thermal and LiDAR imagery using drones

PUBLICATIONS

Bernhardt, J., Snellings, J., Smiros, A., Bermejo, I., **Rienzo, A.**, & Swan, C. (2019). Communicating Hurricane Risk with Virtual Reality: A Pilot Project, *Bulletin of the American Meteorological Society*, 100(10), 1897-1902. https://journals.ametsoc.org/view/journals/bams/100/10/bams-d-17-0326.1.xml

PRESENTATIONS

Rienzo, A., Deeb, E., Vuyovich, C., Duffy, G., Tuttle, S., 2022. Comparing passive microwave snowmelt detection methods using ground-based snowmelt observations. *Eastern Snow Conference*, Easton, PA. Poster presentation.

Rienzo, A., Deeb, E., Vuyovich, C., Duffy, G., Tuttle, S., 2022. Interpreting Snowmelt Events from Passive Microwave Observations. *American Geophysical Union Fall 2022 Conference*, Chicago, IL. Oral presentation.

Rienzo, A., Deeb, E., Vuyovich, C., Tuttle, S., 2022. Evaluating Passive Microwave Snowmelt Detection Methods with Ground Snow Observations. *CMOS-CGU-Eastern Snow Conference Joint Congress*, virtual.

Rienzo, A., Deeb, E., Vuyovich, C., Tuttle, S., 2022. Evaluating Passive Microwave Snowmelt Detection Methods with Ground Snow Observations. *Central New York Earth Science Student Symposium,* Syracuse, NY. Poster Presentation.

Rienzo, A., Roscoe, S., Mahoney, L., Weinstein, P., Tsakiri, K., Petrocheilos, C., Marsellos, A., 2019. Time Series Analysis Comparing Climatic Averages and the Water Levels of Aquifers in Albany, NY and Queens, NY. 26th Conference of *Geology of Long Island and Metropolitan New York (LIG)*, Stony Brook, NY. Extended abstract and poster presentation.

Rienzo, A., 2019. Communicating Hurricane Risk with Virtual Reality: A Demographic Study. *Annual Meeting of the American Association of Geographers (AAG)*, Washington, D.C. Poster Presentation.

Rienzo, A., Bernhardt, J., 2018. Communicating Hurricane Risk with Virtual Reality. *AAG, Middle States Division Annual Meeting*, Montclair, NJ. Poster Presentation.

Rienzo, A., Bernhardt, J., Bermejo, I., 2018. Communicating Hurricane Risk with Virtual Reality: A Student Perspective. *Annual Meeting of the American Association of Geographers (AAG)*, New Orleans, LA. Oral Presentation.

Rienzo, A., Mecca, K., Weinstein, P., Marsellos, A.E. Ph.D., 2018. Multiple Flooding Locations in Oneida County, NY in 2017: An Approach to Determine Flood Vulnerable Sites using LiDAR in Geographical Information Systems (GIS) and Flood Simulations. *10th Annual Mohawk Watershed Symposium*, Schenectady, NY. Extended abstract and poster presentation.

Rienzo, A., Swan, C., Bernhardt, J. Ph.D., 2018. Communicating Hurricane Risk with Virtual Reality: A Pilot Study. *43rd Annual Northeastern Storm Conference*, Saratoga Springs, NY. Poster Presentation.

SEMINARS AND SHORT COURSES

CUAHSI/NASA Snow Measurement Field School – Heber City, UT ***March 2023***

- 5-day field training in 6ft deep snowpack: snow safety, measurement techniques and instrumentation, planning field campaigns/sampling design, and data analysis.

SnowEx Hack Week 2022 ***July 2022***

- Attended various seminars on SnowEx mission and datasets, snow remote sensing, data analysis, and Python training
- Collaborated with individuals of diverse experience to create a pipeline to 1) connect SNOTEL stations to relevant SnowEx datasets and 2) investigate snow variability of SNOTEL station data due to land heterogeneity

TEACHING EXPERIENCE

Teaching Assistant, Earth Science Laboratory and Recitation ***Fall 2020***
Department of Earth and Environmental Sciences, Syracuse University

- Lead weekly laboratory exercises for three course sections of 25+ students each
- Lead separate recitation section with weekly Google Earth Pro exercises
- Graded 75+ student assignments weekly

Tutor, **Introduction to Geology** ***Fall 2018 – Spring 2020***
Department of Geology, Hofstra University

- Provided extra aid to students enrolled in the Introductory Geology course
- Prepared students for tests and quizzes through extra instruction and practice

OUTREACH AND SERVICE

6th Grade Geoscience Outreach – Clark Reservation State Park, NY ***May 2023***

- Designed immersive/hands-on activities to teach students about water cycle, soil infiltration, and ground water.
- Co-taught ~18 groups of 10-15 6th grade students over a 3-day event

Treasurer Secretary - Geology Graduate Student Organization ***Fall 2022 – May 2023***
Elected by Geology Graduate Student body, Syracuse University

- Manage finances of the organization and promote transparency, discussion, and best choices about how to spend funds
- Assist in funding, planning, and execution of graduate student run *Central NY Earth Science Student Symposium*

DEI Committee Member ***Fall 2022 – present***
Department of Earth and Environmental Sciences, Syracuse University

- Assist with planning and execution of events aimed at promoting diversity, equity, and inclusion within the graduate student population in the department, such as workshops, invited seminars, and reading groups

GRANTS, AWARDS, AND FUNDING

Research Assistantship *Syracuse University* ***Spring 2021 – present***
Teaching Assistantship *Syracuse University* ***Fall 2021***
Award for Academic Excellence in Geology *Hofstra University* ***2019***
HU Honors College Research Assistantship *for undergraduate research* ***Fall 2017***

Provost's Scholar ***Fall 2017 – Spring 2020***
Dean's Scholar ***Fall 2016 – Spring 2017***
Presidential Scholar *Hofstra University* ***Fall 2016 – Spring 2020***

TECHNICAL SKILLS

Programming/Programs: R, Python, Excel, SPSS, Knime, GitHub
Spatial Analysis: ArcGIS Pro, ArcMap, QGIS, Google Earth Pro, Global Mapper
Visualization: Adobe Illustrator, cartographic design
Microsoft Office Suite: PowerPoint, Word, Excel

PROFESSIONAL MEMBERSHIPS

American Geophysical Union ***Member; 2022 – present***
American Association of Geographers ***Member; 2017 – 2020***
Sigma Gamma Epsilon ***Vice President; 2019 – 2020***
- National Honors Society for Earth Sciences, HU Chapter